



A RE-ENTRY CONTROL SYSTEM USING  
DELTA-MODULATED ACCELEROMETERS  
AND A DDA-COMPUTER

by

HANS-FREDRIK MILLERS

Civilingenjör, Chalmers Tekniska Högskola,  
Göteborg, Sweden, 1957

SUBMITTED IN PARTIAL FULFILLMENT OF THE  
REQUIREMENTS FOR THE DEGREE OF  
MASTER OF SCIENCE

at the

MASSACHUSETTS INSTITUTE OF TECHNOLOGY

August, 1964

Signature of Author Hans-Fredrik Millers  
Department of Aeronautics and Astronautics, August, 1964

Certified by Wallace E Vande Veldt  
Thesis Supervisor

Accepted by Carl Killip  
Chairman, Departmental Graduate Committee



A RE-ENTRY CONTROL SYSTEM USING  
DELTA-MODULATED ACCELEROMETERS  
AND A DDA-COMPUTER

by

HANS-FREDRIK MILLERS

Civilingenjör, Chalmers Tekniska Högskola,  
Göteborg, Sweden, 1957

SUBMITTED IN PARTIAL FULFILLMENT OF THE  
REQUIREMENTS FOR THE DEGREE OF  
MASTER OF SCIENCE

at the

MASSACHUSETTS INSTITUTE OF TECHNOLOGY

August, 1964

Signature of Author

Signature redacted

Department of Aeronautics and Astronautics, August, 1964

Certified by

Signature redacted

Thesis Supervisor

Accepted by

Signature redacted

Chairman, Departmental Graduate Committee

A RE-ENTRY CONTROL SYSTEM USING  
DELTA-MODULATED ACCELEROMETERS  
AND A DDA-COMPUTER

by

HANS-FREDRIK MILLERS

Submitted to the Department of Aeronautics and Astronautics on August 24, 1964, in partial fulfillment of the requirements for the degree of Master of Science.

ABSTRACT

This thesis is concerned with the problem of controlling a lifting re-entry vehicle during the atmospheric phase characterized by subcircular velocity. The vehicle under investigation is a constant trim (constant  $L/D$ ) vehicle. The control problem is divided into two sub-problems. One is the range control and the other is the lateral control.

Approximate expressions for the nominal trajectory are given and the long period motion of the vehicle is derived using linearization at local points along the trajectory.

The range control system uses the nominal trajectory as a reference and controls the range by adjusting the vertical component of the lift-to-drag ratio which is achieved by rolling the vehicle. An accelerometer package consisting of three delta modulated accelerometers measures the acceleration and a DDA computer performs the necessary calculations. The delta modulated accelerometer is described and special attention is paid to the limit cycle problem in the range control loop due to the output character of the delta modulated accelerometer. A low frequency model is derived for the accelerometer. During the first part of the analyzed flight the range control experiences a limit cycle, which dies out as the vehicle approaches the landing point. No analysis regarding initial errors is carried out.

The lateral control system operates as an on-off system switching the lift vector from one side to the other to keep the cross range error within desired limits. The limit cycle of the lateral control is analyzed using the phase plane method.

Thesis Supervisor: Wallace E. Vander Velde, Sc. D.

Associate Professor of  
Aeronautics and Astronautics

## ACKNOWLEDGMENT

The author is grateful to Professor Wallace E. Vander Velde for the guidance he has given as thesis supervisor during the progress of this report.

In addition, Miss Janice Kelley performed heroically in typing the thesis.

## TABLE OF CONTENTS

CHAPTER 1.	INTRODUCTION	1
1.1	Object	1
1.2	Reentry Philosophy	1
1.3	Range and Lateral Control Systems	4
1.4	Guidance Equipment	5
CHAPTER 2.	NOMINAL TRAJECTORY	7
2.1	Introduction	7
2.2	Equations of Motion	7
2.3	Solution of the Equations of Motion	9
2.4	Some Useful Expressions	14
2.5	Remarks	16
CHAPTER 3.	VEHICLE DYNAMICS	17
3.1	Introduction	17
3.2	The Perturbation Equations	17
3.3	The Vehicle Transfer Functions	23
CHAPTER 4.	DELTA -MODULATED ACCELEROMETERS AND DIGITAL DIFFERENTIAL ANALYZER	33
4.1	Introduction	33
4.2	Delta -Modulated Loops	34
4.2.1	Description of the Loop	34
4.2.2	Describing Function Analysis	36
4.3	Delta -Modulated Accelerometer	38
4.4	Delta -Modulated Accelerometer with Three -Level Relay	42
4.5	Increment Size and Clock Frequency	45
4.6	A Non -Linear Model for the Delta -Modulated Accelerometer	46
4.7	DDA -Computer	49

## CONTENTS

CHAPTER 5.	RANGE CONTROL	53
5.1	Introduction	53
5.2	The Range Control System and its Stabilization	53
5.3	Introduction of a Delta-Modulated Accelerometer and a DDA-Computer in the Range Control Loop	59
5.4	Limit Cycles	62
CHAPTER 6.	LATERAL CONTROL	71
6.1	Introduction	71
6.2	The Lateral Control System	71
6.3	Maximum Initial Errors that Can Be Corrected	81
CHAPTER 7.	SUMMARY AND CONCLUSIONS; SUGGESTIONS FOR FURTHER STUDY	85
7.1	Summary and Conclusions	85
7.2	Suggestions for Further Study	87
REFERENCES		88
APPENDIX		
A.1	Delta-Modulation Loop with Two Level Relay	93
A.2	Delta-Modulation Loop with Three Level Relay	95
A.3	Control Loop for a Delayed Modulated Input	97
A.4	3-Level Modulation Loop	99
A.5	Modulation	104
A.6	Frequency Response of a Linear Single Axis Positioner	111
A.7	Error of a Manual Accelerometer	117
A.8	Delta-Modulated Accelerometer with Three Level Relay	121
A.9	Delta-Modulated Accelerometer plus Integrator	127
A.10	Linear Error Model of Delta-Modulated Accelerometer	131
A.11	Comparison of methods	133
A.12	Requisite Assignment of DDA-Integrator	134
A.13	Requisite Compensation of DDA-Integrator	134
A.14	DDA-System for Formation	134
A.15	DDA-System for Formation by a Constant	134
CHAPTER 8		
8.1	Range Control System	144
8.2	Block Diagram of Range Control System	152
8.3	Summary	154

## LIST OF FIGURES

CHAPTER 1		
1.1	Guidance in Supercircular Entries	3
CHAPTER 2		
2.1	The Two-Dimensional Trajectory	8
CHAPTER 3		
3.1	The xyz-Coordinate System	24
3.2	The Coordinate Systems XYZ and xyz	25
3.3	Block Diagram for $\Delta r$	28
3.4	Simplified $\Delta r$ -Block Diagram	28
3.5	Block Diagram for $\Delta V$	31
3.6	Simplified $\Delta V$ -Block Diagram	31
CHAPTER 4		
4.1	Delta-Modulated Loop with Two Level Relay	35
4.2	Delta-Modulated Loop with Three Level Relay	35
4.3	Sampler Output for a Delayed Sinusoid Input	37
4.4	A Delta-Modulated Loop	38
4.5	Moding Plot	39
4.6	Pictorial Diagram of Floated Single-Axis Pendulum	41
4.7	Delta-Modulated Accelerometer	42
4.8	Delta-Modulated Accelerometer with Three Level Relay	42
4.9	Delta-Modulated Accelerometer plus Integrator	47
4.10	Low Frequency Model of Delta-Modulated Accelerometer	47
4.11	Describing Function	50
4.12	Register Arrangement of DDA-Integrator	51
4.13	Schematic Representation of DDA-Integrator	51
4.14	DDA-Symbol for Summation	51
4.15	DDA-Symbol for Multiplication by a Constant	51
CHAPTER 5		
5.1	Range Control System	54
5.2	Block Diagram of Range Control System	55
5.3	Inner Loop	56

## FIGURES

5.4	Root Locus for Inner Loop, $\bar{V} = 0.30$	56
5.5	Root Locus for Inner Loop, $\bar{V} = 0.90$	56
5.6	Outer Loop	57
5.7	Root-Locus for Outer Loop, $\bar{V} = 0.30$	58
5.8	Root-Locus for Outer Loop, $\bar{V} = 0.90$	58
5.9	Range Control Loop with DMA and DDA	60
5.10	Illustration of DDA -Program	60
5.11	Range Control Loop with Delta -Modulated Accelerometer	63
5.12	Low Frequency Model of Range Control Loop	66
5.13	Range Control for $\bar{V} = 0.90$	67
5.14	Range Control for $\bar{V} = 0.30$	68

## CHAPTER 6

6.1	Lateral Flight Path	72
6.2	Prediction of Cross Range Error	73
6.3	Lateral Control System	74
6.4	Block Diagram for Phase Plane Analysis	75
6.5	Phase Plane for $\bar{V} = 0.30$	78
6.6	Phase Plane for $\bar{V} = 0.90$	79
6.7	Lateral Trajectory	82
6.8	Cross Range Error Due to Initial Errors	82
6.9	Acceptable Initial Errors	83



## LIST OF SYMBOLS

- A Reference area of vehicle.  
Amplitude of sinusoid input to non-linearity.
- $A_C$  Half-width of zero level of relay in delta modulated loop.
- $A_{OA}$  Angle through which instrument float has turned with respect to the case about its output axis.
- $a_{IA}$  Acceleration of accelerometer with respect to inertial space along its input axis.
- $a_{max}$  Maximum acceleration system will experience.
- B Bank angle.
- C Damping coefficient of fluid damper output from DDA.
- $C_D$  Drag coefficient.
- D Drag force.  
Drive level of relay.  
Transfer function of DDA.
- E Allowable error in range.
- e Output signal from relay.
- F Force.
- f Frequency of accelerometer clock.
- G Transfer function.
- $G_{oh}$  Zero order hold.
- g Magnitude of gravitational acceleration.
- h Altitude.
- I. M. Impulse modulator.

J	Moment of inertia about accelerometer output axis.
K	Universal gravitational constant. DDA -constant.
L	Lift force.
$l$	Lateral range, measured from initial trajectory plane.
$l_0$	Maximum possible lateral range.
$l_m$	Allowable cross range error.
$l_f$	Predicted cross range error.
M	Mass of earth. Torque level of torque generator.
$M_{tg}$	Torque applied by torque generator.
$N(A, \omega)$	Describing function.
n	Integer.
P	Pendulosity of accelerometer.
p	Integer.
R	Remainder in DDA. Down range.
$r_p$	Mean radius of earth.
S	Distance measured along flight path.
s	Laplace variable.
T	Total time of flight.
$T_n$	Navigation time.
$T_s$	Sampling time.
t	Time.
U	DDA -Signal.
V	Magnitude of velocity with respect to non-rotating coordinate system DDA -signal.

$\bar{V}$	Velocity divided by local circular orbital velocity.
$V_{in}$	Velocity input to accelerometer model.
$V_{out}$	Velocity output from accelerometer model.
$V_s$	Local circular orbital velocity.
$\delta V$	Velocity increment.
$X$	Distance measured along surface of earth.
xyz	Coordinate system.
XYZ	Coordinate system.
$z$	Z-transform variable, $z = e^{sT_s}$ .
$\beta$	Exponential decay constant of atmosphere.
$\gamma$	Flight path angle measured with respect to local geographic horizontal.
$\Delta$	Difference when linearizing.
$\epsilon$	Angle of coordinate rotation.
$\zeta$	Relative damping.
$\theta$	Angular range in trajectory plane.
$\rho$	Atmospheric density.
$\rho_0$	Constant of atmospheric density model.
$\tau$	Time constant. Normalized time.
$\phi$	Maximum phase shift due to sampling delay for mode n-n.
$\varphi$	Roll angle.
$\psi$	Heading angle from trajectory plane.
$\omega$	Angular frequency.
$\omega_n$	Natural frequency.
$\omega_{orb}$	Orbital angular velocity.

- $\omega_s$  Sampling frequency.
- $\omega_0$  Natural frequency of long period motion.  
Time normalizing constant for phase plane design.

### Subscripts

- i Initial value
- f Final value
- h Horizontal component
- v Vertical component
- n Nominal value
- IA Input axis
- OA Output axis
- xyz Components along the coordinate axes, xyz
- XYZ Components along the coordinate axes, XYZ

## CHAPTER 1

### INTRODUCTION

#### 1.1 Object

During the past decade interest in space travel has increased tremendously and a trip to another planet is today far from science fiction. The first step of space travel to be made by this country is the Apollo project, whose object is to land two men on the moon and then pick them up and bring the space crew back to the earth. There are, of course, many problems to be solved before a manned spacecraft can safely be sent out from the earth with hope to get the crew back. One problem common to all space travel is how a returning spacecraft should be landed on the earth.

This thesis is concerned with the problem of controlling a lifting vehicle through the atmosphere to a desired point when Delta Modulated Accelerometers are used to measure acceleration and a Digital Differential Analyzer, DDA, is used for the computations.

#### 1.2 Reentry Philosophy

The reentry vehicle under investigation in this thesis is without thrust so that the only force available to control the trajectory is aerodynamic. The shape of the vehicle is further, such that the vehicle will experience a constant lift-to-drag ratio. The only way to control the trajectory is therefore to roll

the vehicle and with it the lift vector, which can be achieved by small roll jets.

When landing a vehicle on the earth several requirements must be met. Among other things, the acceleration and heating loads must be kept within design limits in order to assure the vehicle's arrival at the desired destination. The space vehicle is approaching the atmosphere of the earth with a small angle and the method suggested to break down the supercircular velocity of the vehicle and landing it is shown in Fig. 1.1.

During the first phase of the landing, up to point A in Fig. 1.1, the vehicle has its lift vector pointing upwards. When the flight path starts to pull up at point A the vehicle goes into a climb which is a controlled flight to prevent escape. At point B a constant altitude phase begins. The atmosphere has continuously decelerated the speed of the vehicle and at the end of the constant altitude phase, point C, the velocity is subcircular, and the altitude about 300,000 ft. From this point up to a point very close to the destination point the nominal flight trajectory is defined by a constant lift-to-drag ratio with the lift vector in the vertical plane pointing out from the earth as shown in Fig. 1.1. The last part from D to the destination point can be handled by conventional techniques as the velocity now is less than a fifth of the circular velocity and the vehicle is in high density atmosphere.

In this paper the control of the trajectory from C to D will be studied and this phase of the reentry will, in the following, be called the Landing Phase.

In Chapter 2 the predicted range to go for a constant lift-to-drag ratio vehicle is derived. The result shows that the range to go is proportional to the lift-to-drag ratio. Other studies, Ref. (1) and (2), have proved that the

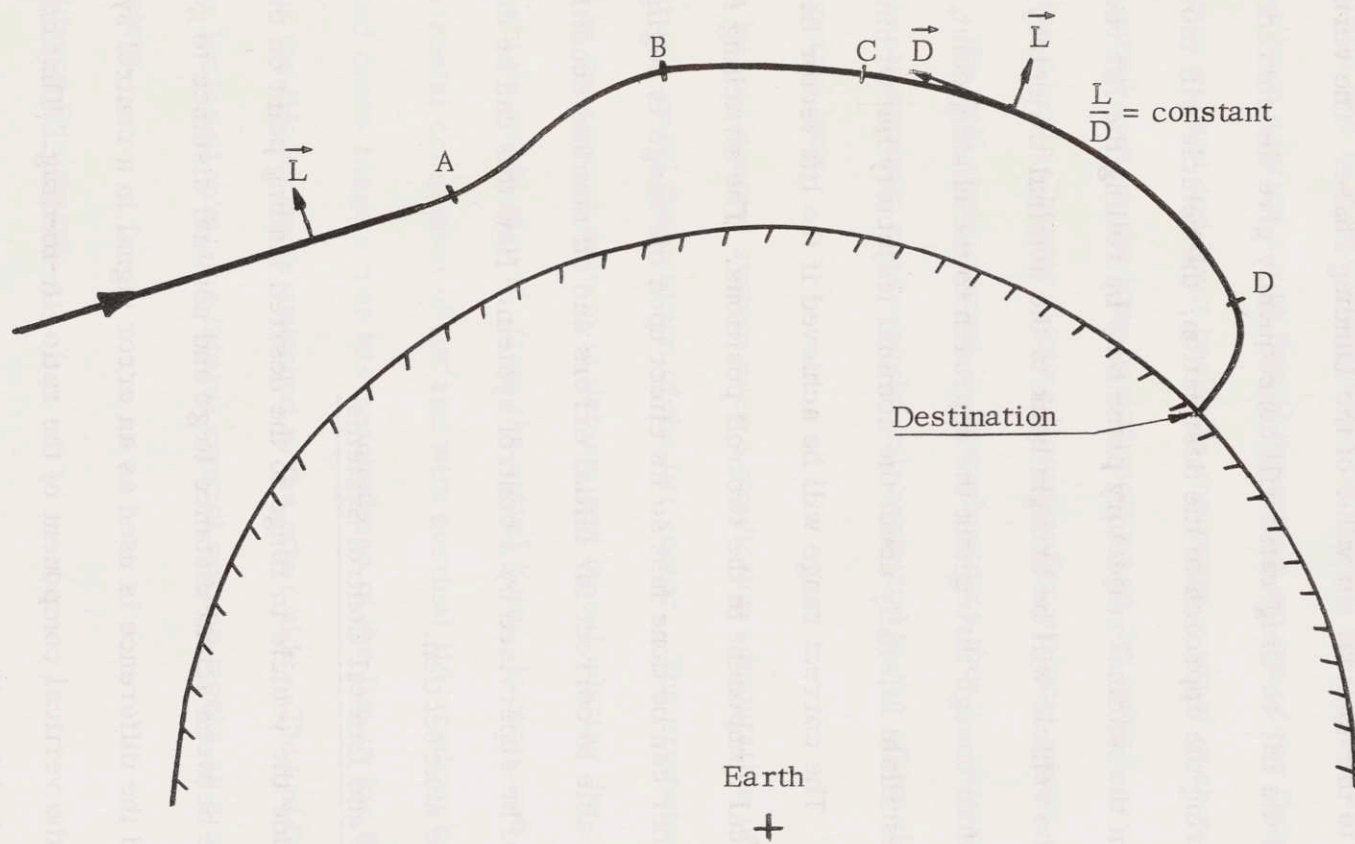


Fig. 1.1 Guidance in Supercircular Entries.

cross coupling between longitudinal and lateral motion can be neglected when the lift vector is rolled out from the vertical plane. That gives a natural method of controlling the vehicle during the Landing Phase. If the vehicle is designed with a lift vector larger than the nominal value for the Landing Phase, the lift vector may be rolled out from the vertical plane so that the vertical component of lift corresponds to the nominal lift value of the Landing Phase. The vertical component of the lift-to-drag ratio will consequently give the correct range. However, during the approach to the destination, the vehicle will move out laterally from the nominal trajectory plane but, by rolling the lift vector to the other side, the vehicle will be brought back to the nominal trajectory. If this is repeated often enough throughout the approach to the landing point, the vehicle will oscillate laterally about the nominal trajectory but within the cross range limits. The correct range will be achieved if the lift vector has the correct vertical component in the two roll positions. The switching from one side to the other can be done fast so its effect upon the range is negligible.

To be able to correct for initial errors and off nominal conditions the vehicle should be supervised by a control system. How this can be done is outlined in the next section.

### 1.3 Range and Lateral Control Systems

To guide the vehicle in range to the desired landing point on the earth the difference between actual distance to go and nominal distance to go are compared and the difference is used as an error signal in a control system operating on the vertical component of the ratio lift-to-drag. That component of the lift-to-drag ratio is controlled by rolling the vehicle a small angle proportional to the command signal. To stabilize the range control system



signals other than the error in the range have to be introduced. In this paper the acceleration and velocity error in the direction along the nominal flight path are used as stabilizing signals. The acceleration in that direction is measured by an accelerometer package mounted on an inertial platform. The accelerometer package consists of three Delta-Modulated Accelerometers whose pulses are transmitted to a DDA-computer which performs the necessary computations. Analysis has been carried out to find if the output nature of the Delta-Modulated Accelerometer causes any limit cycles in the range control system. To design the range control system the long period motions of the vehicle must be derived. This has been done in Chapter 3 using linearization at local points along the trajectory. The roll angle control is, throughout this thesis, assumed to have a bandwidth so its dynamic can be neglected compared to the other elements in the range control loop.

The lateral control system uses a prediction computation of the cross range error to control the position of the lift vector. The predicted cross range error used in the control system is determined by calculating the cross range error the vehicle would give if, from the actual point, it continued its flight without horizontal component of lift and with nominal lift-to-drag ratio. When the predicted cross range error has reached one of the limits for the cross range error the lift vector is switched to the other side. This is then repeated at the other limit and thus, the lateral control system works as a two position control system.

#### 1.4 Guidance Equipment

The vehicle is equipped with a Space Integrator (inertial platform) which, in this thesis, is assumed to carry a package of three Delta Modulated Accelerometers.

meters. The accelerometer outputs are resolved by the vehicle computer to yield the desired components. Prior to the reentry the Space Integrator is aligned and then holds its orientation relative to inertial space.

The choice of computer is defined by the overall mission and in most cases a general purpose digital computer would be chosen. In this thesis, however, the reentry control is treated as a separate problem and a DDA-computer has been chosen for the computations and the analysis to be carried out.

Both the Delta-Modulated Accelerometer and the DDA-computer have been described in the literature, i. e., Refs. (3), (4), (5), and (6).

## CHAPTER 2

### NOMINAL TRAJECTORY

#### 2.1 Introduction

Before it is possible to start analyzing the overall control system of the range control, several pre-calculations must be done. One of these is to determine the characteristics of the nominal trajectory during the landing phase. The nominal trajectory of that phase of the re-entry has a constant L/D and the equilibrium glide path is essentially that one where the aerodynamic lift force just balances the centrifugal and gravity force along the trajectory. The initial conditions required are a near-horizontal entry angle and a velocity slightly below circular orbital velocity.

A general analytic expression describing the motion of a body moving through a planetary atmosphere does not exist. However, several authors, i. e., Refs. (1), (7), and (8), have derived approximate solutions. The derivations in this chapter will follow the general pattern.

#### 2.2 Equations of Motion

Using the notations of Fig. 2.1 we can write the differential equations of motion. The first equation defines the motion perpendicular to the flight path and the second parallel to the flight path

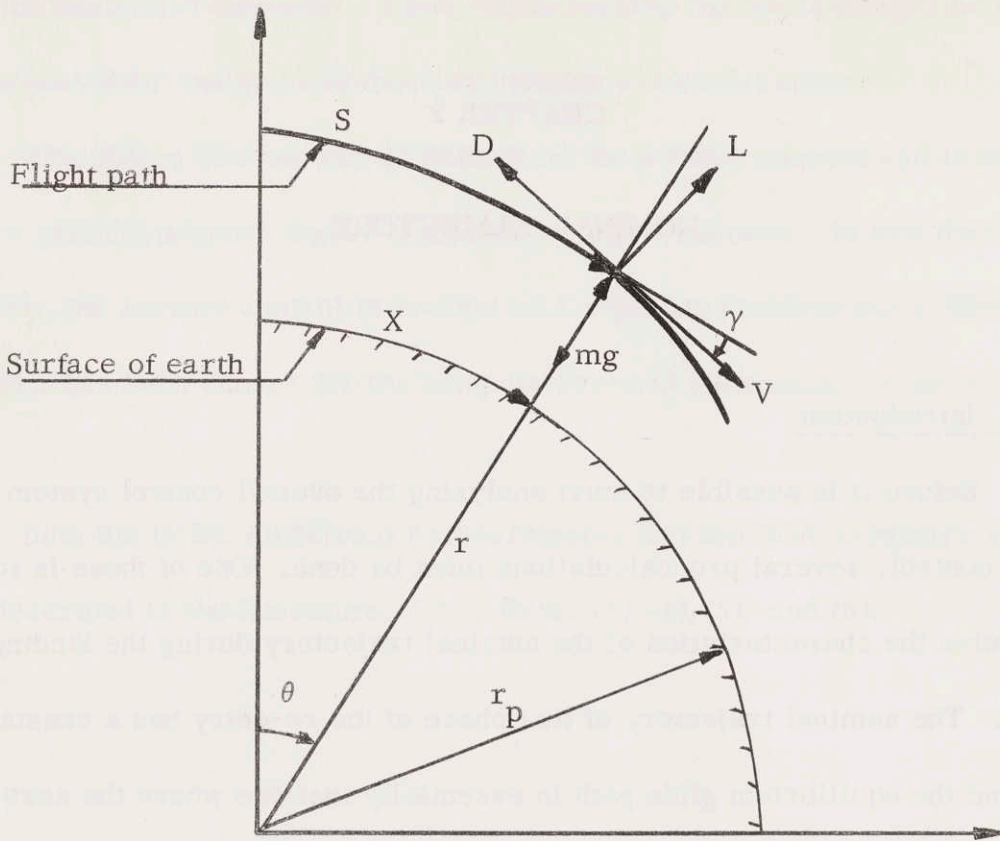


Fig. 2.1 The Two-Dimensional Trajectory.

Notations:	$\theta$	angular range
	V	velocity measured with respect to an inertial coordinate system
	m	mass
	D	drag
	L	lift
	g	local gravitational acceleration
	r	distance to the center of the planet
	$r_p$	radius of the planet
	$\gamma$	flight path angle with respect to local geographic horizon
	S	distance along flight path
	X	distance along surface
	h	$(r - r_p)$

$$\frac{V^2 \cos \gamma}{r} + V\dot{\gamma} = g \cos \gamma - \frac{L}{m} \quad (2.1)$$

$$\frac{dV}{dt} = g \sin \gamma - \frac{D}{m} \quad (2.2)$$

When writing the equations of motion it has been assumed that the planet and the atmosphere are not rotating and also that the planet is spherical. Fig. 2.1 shows that the rate of change of the altitude is a function of velocity and flight path angle

$$\frac{dh}{dt} = -V \sin \gamma \quad (2.3)$$

The traveled distance along the surface is related to velocity and flight path angle as follows:

$$\frac{dX}{dt} = \frac{r}{p} V \cos \gamma \quad (2.4)$$

### 2.3 Solution of the Equations of Motion

To be able to get the solutions of the equations of motion in a nice analytic form, some approximations must be done. The flight path angle will be small so that  $\cos \gamma = 1$ . If we then neglect  $V\dot{\gamma}$  and the component of gravity along the flight path compared to the drag, equations (2.1) and (2.2) become

$$\frac{V^2}{r} = g - \frac{L}{m} \quad (2.5)$$

$$\frac{dV}{dt} = -\frac{D}{m} \quad (2.6)$$

Equations (2.5) and (2.6) will give analytic solutions.

When solving the equations of motion it is preferable to choose a ratio of velocity to local circular orbital velocity as independent variable instead of the velocity itself. If denoting the ratio by  $\bar{V}$ , and the local circular orbital velocity by  $V_s$ , the ratio is

$$\bar{V} = \frac{V}{V_s} \quad (2.7)$$

where

$$V_s^2 = gr$$

Substituting the ratio  $\bar{V}$  into the equations (2.5) and (2.6) yields

$$\frac{V_s^2}{r} (1 - \bar{V}^2) = \frac{L}{m} \quad (2.8)$$

$$V_s \frac{d\bar{V}}{dt} = -\frac{D}{m} - \bar{V} \frac{dV_s}{dt} \quad (2.9)$$

If eliminating  $m$  by substituting equation (2.8) into (2.9), it will result in the following differential equation

$$V_s \frac{d\bar{V}}{dt} = -\frac{V_s^2}{r} \frac{L}{D} (1 - \bar{V}^2) - \bar{V} \frac{dV_s}{dt} \quad (2.10)$$

The acceleration along the trajectory may be written as

$$\frac{dV}{dt} = \frac{dV}{dS} \cdot \frac{dS}{dt} = \frac{dV}{dS} \cdot V \quad (2.11)$$

Assuming  $V_s$  a constant and dividing both sides of equation (2.11) by  $V_s$  gives

$$\frac{d\bar{V}}{dt} = V_s \bar{V} \frac{d\bar{V}}{dS} \quad (2.12)$$

Substituting equation (2.12) into equation (2.10) and again neglecting the rate of change of the circular orbital velocity transforms equation (2.10) to

$$V_s^2 \bar{V} \frac{d\bar{V}}{dS} = - \frac{V_s^2}{r \frac{L}{D}} (1 - \bar{V}^2) \quad (2.13)$$

or

$$dS = \frac{-r \frac{L}{D} \bar{V} d\bar{V}}{(1 - \bar{V}^2)} \quad (2.14)$$

Equation (2.14) can easily be integrated if assuming  $L/D$  to be a constant and  $r$  to be equal to a mean radius  $r_m$  of the trajectory. The distance along the flight path is then

$$S_f - S_i = \frac{1}{2} r_m \frac{L}{D} \ln \left[ \frac{1 - \bar{V}_f^2}{1 - \bar{V}_i^2} \right] \quad (2.15)$$

where the subscripts  $i$  and  $f$  denote initial and final values, respectively.

When the velocity has decreased to  $\bar{V} = 0.4$  a distance of 95% of the total one has already been covered. If the final velocity is taken to be very small, it is therefore possible to neglect  $\bar{V}_f$  in equation (2.15). The expression for the total range  $S$  becomes then

$$S = \frac{1}{2} r_m \frac{L}{D} \ln \frac{1}{1 - \bar{V}_i^2} \quad (2.16)$$

Distance traveled along the flight path can be translated to distance traveled along the ground by the expression

$$X = \frac{r_p}{r_m} S \quad (2.17)$$

or to angular range  $\theta$ , as shown in Fig. 2.1, by the formula

$$\theta = \frac{1}{2} \frac{L}{D} \ln \frac{1}{1 - \bar{V}_i^2} \quad (2.18)$$

which is independent of radius and proportional to  $L/D$ .

It is important to know the flight path angle. To be able to derive an expression for the flight path angle the altitude must first be calculated along the flight path. This can be done by use of equation (2.8) and the knowledge of the altitude-density relationship of the earth. The conventional approximation of the density as a function of altitude is

$$\rho = \rho_0 e^{-\beta h} \quad (2.19)$$

where  $\rho$  is the density and  $\rho_0$  and  $\beta$  are constants ( $\rho_0 = 0.0027 \text{ slug/ft}^3$  and  $\beta = \frac{1}{23500} \text{ ft}^{-1}$ ). The approximation is good below 300,000 feet.

The lifting force is

$$L = \frac{1}{2} \rho \bar{V}^2 V_s^2 C_L A \quad (2.20)$$

where  $C_L$  and  $A$  represents lift coefficient and a reference area, respectively. Substituting equation (2.20) into equation (2.8) and solving for  $\rho$  yields

$$\rho = \frac{2(1 - \bar{V}^2)}{\frac{C_L A}{m} \cdot r \bar{V}^2} \quad (2.21)$$

The expression for the altitude is then given by equation (2.19) and (2.21)

$$h = \frac{1}{\beta} \ln \frac{\rho_0 \frac{C_L A}{m} r \bar{V}^2}{2(1 - \bar{V}^2)} \quad (2.22)$$



Figure 2.1 shows that the equilibrium glide flight path angle is

$$\gamma = -\frac{\frac{dh}{dt}}{V} = -\frac{\frac{dh}{d\bar{V}} \cdot \frac{d\bar{V}}{dt}}{\bar{V}V_s} \quad (2.23)$$

If  $C_L$ ,  $r$  and  $\beta$  are assumed to be constant, equation (2.22) can be differentiated to get  $dh/d\bar{V}$ . Equation (2.10) gives  $d\bar{V}/dt$ , then equation (2.23) takes the form

$$\gamma = \frac{2}{r\beta\bar{V}^2} \frac{L}{D} \quad (2.24)$$

The line of travel along the trajectory can be calculated from equation (2.10) if  $V_s$  is assumed to be a constant as before. Separating the variables of equation (2.10) yields

$$dt = -\frac{r \frac{L}{D} d\bar{V}}{V_s (1 - \bar{V}^2)} \quad (2.25)$$

If equation (2.25) is integrated, assuming  $r$ ,  $V_s$  and  $L/D$  constant, the result is

$$t_f - t_i = \frac{r \frac{L}{D}}{2V_s} \left[ \ln \frac{1 + \bar{V}_i}{1 - \bar{V}_i} - \ln \frac{1 + \bar{V}_f}{1 - \bar{V}_f} \right] \quad (2.26)$$

As the final velocity is very small, the total time  $T$  may be approximated as follows:

$$T = \frac{r \frac{L}{D}}{2V_s} \ln \frac{1 + \bar{V}_i}{1 - \bar{V}_i} \quad (2.27)$$

## 2.4 Some Useful Expressions

In this section some expressions will be derived which are needed in the following chapters when calculating the perturbation equations for the flight path dynamics. The derivatives of the perturbation equations are all functions of the nominal flight path characteristics.

Equation (2.25) gives the dimensionless acceleration

$$\frac{d\bar{V}}{dt} = - \frac{V_s (1 - \bar{V}^2)}{r \frac{L}{D}} \quad (2.28)$$

and if  $V_s$  is assumed to be constant, the acceleration along the flight path takes the form

$$\frac{dV}{dt} = - \frac{V_s^2 (1 - \bar{V}^2)}{r \frac{L}{D}} \quad (2.29)$$

However,  $V_s$  and  $r$  are related to each other as follows:

$$V_s = \sqrt{gr} \quad (2.30)$$

and

$$\omega_{orb}^2 = \frac{V_s^2}{r} = \frac{g}{r} \quad (2.31)$$

where  $\omega_{orb}$  is local orbital frequency. Substituting equation (2.30) into equation (2.29) yields

$$\frac{dV}{dt} = - \frac{g(1 - \bar{V}^2)}{\frac{L}{D}} \quad (2.32)$$

The acceleration along the nominal flight path is thus primarily a function of  $\bar{V}$  and  $L/D$ .

Figure 2.1 gives the rate of change of  $r$

$$\frac{dr}{dt} = -V\gamma \quad (2.33)$$

The flight path angle  $\gamma$  is given by equation (2.24). Substituting that equation into equation (2.33) transforms (2.33) to

$$\frac{dr}{dt} = - \frac{2V_s^2}{r\beta V \cdot \frac{L}{D}} \quad (2.34)$$

or

$$\frac{dr}{dt} = - \frac{2V_s^2}{r\beta \bar{V} \frac{L}{D}} \quad (2.35)$$

The second derivative of  $r$  or altitude can be calculated from equation (2.34) by derivation

$$\frac{d^2r}{dt^2} = \frac{2V_s^2}{rV\beta \frac{L}{D}} \cdot \left[ \frac{1}{V} \frac{dV}{dt} + \frac{1}{r} \frac{dr}{dt} \right] \quad (2.36)$$

Substituting equation (2.32) and (2.34) into equation (2.36) gives

$$\frac{d^2r}{dt^2} = - \frac{2g}{r\beta \bar{V}^2 \left(\frac{L}{D}\right)^2} \left[ 1 - \bar{V}^2 + \frac{2}{\beta r} \right] \quad (2.37)$$

As  $\beta r \approx 10^3$ , equation (2.37) may be approximated to

$$\frac{d^2r}{dt^2} = - \frac{2g}{r\beta \left(\frac{L}{D}\right)^2} \cdot \frac{1 - \bar{V}^2}{\bar{V}^2} \quad (2.38)$$

The second derivative is thus rapidly increasing for decreasing  $\bar{V}$ . It is also of interest to know the drag and lift forces along the equilibrium glide path.

Substituting equation (2.32) into equation (2.6) gives the drag force.

$$D = m \cdot \frac{g(1 - \bar{V}^2)}{\left(\frac{L}{D}\right)} \quad (2.39)$$

The drag force is a function of the dimensionless velocity and the L/D ratio for the flight path. Solving equation (2.39) for the lift force results in

$$L = m \cdot g(1 - \bar{V}^2) \quad (2.40)$$

The lift force is just a function of the dimensionless velocity.

### 2.5 Remarks

The equations derived here for the nominal trajectory are of course not exact but will serve the purpose of giving nominal characteristics for the perturbation equations in the next chapter very well. The range expression may also be used in a continuous closed loop range control system for the landing where errors in the beginning automatically will be eliminated under the approach to the desired landing point. If an open loop range control is to be used the accuracy of the range expression should be improved. This can be done using the method of adjoint functions described by G. A. Bliss, Ref. (10), and H. S. Tsien, Ref. (11). The adjoint function method has successfully been used by R. Rosenbaum, Ref. (1), for the range prediction problem of a re-entry vehicle entering an atmosphere.

## CHAPTER 3

### VEHICLE DYNAMICS

#### 3.1 Introduction

The next step in building up the range control system is to derive the differential equations describing the dynamics of the vehicle itself. This is best done by linearization of the equations of motion. The nominal trajectory for the linearizations will be the trajectory derived in the preceding chapter. If the linearized model of the vehicle dynamics, during the reentry, will be a good approximation of the line behaviour of the vehicle, depends on the relative change of the coefficients of the differential equations and the bandwidth of the overall system.

#### 3.2 The Perturbation Equations

The perturbation equations will be derived from the complete equations of motion, equations (2.1) and (2.2), which take the following forms if the small angle assumption, with respect to  $\gamma$ , is made

$$\frac{KM}{r^2} - \frac{V^2}{r} - V\dot{\gamma} = \frac{L}{m} \quad (3.1)$$

$$\dot{V} - \frac{KM}{r^2} \gamma = -\frac{D}{m} \quad (3.2)$$

where  $K$  is the universal gravitational constant and  $M$  the mass of the earth.

Replacing  $\gamma$  and  $\dot{\gamma}$  by the relations

$$\gamma = -\frac{\dot{r}}{V} \quad (3.3)$$

$$\dot{\gamma} = -\frac{\ddot{r}}{V} + \frac{\dot{r}\dot{V}}{V^2} \quad (3.4)$$

equations (3.1) and (3.2) become

$$\frac{KM}{r} - \frac{V}{r} + \dot{r} - \frac{\dot{r}\dot{V}}{V} = \frac{L}{m} \quad (3.5)$$

$$\dot{V} + \frac{KM\dot{r}}{r^2V} = -\frac{D}{m} \quad (3.6)$$

To find the deviations about the nominal trajectory introduce the following expressions

$$\begin{aligned} r &= r_n + \Delta r \\ V &= V_n + \Delta V \\ L &= L_n + \Delta L \\ D &= D_n + \Delta D \end{aligned} \quad (3.7)$$

The subscript n denotes the value along the nominal flight path. If equations (3.7) substituted into equations (3.5) and (3.6), the perturbation equations become

$$\begin{aligned} \Delta\ddot{r} - \frac{\dot{V}_n}{V_n} \Delta\dot{r} + \left( \frac{V_n^2}{r_n^2} - \frac{2KM}{r_n^3} \right) \Delta r - \frac{\dot{r}_n}{V_n} \Delta\dot{V} + \\ + \left( \frac{\dot{r}_n \dot{V}_n}{V_n^2} - \frac{2V_n}{r_n} \right) \Delta V = \frac{\Delta L}{m} \end{aligned} \quad (3.8)$$

$$\frac{KM}{r_n^2 V_n} \Delta \dot{r} - \frac{2KM \dot{r}_n}{r_n^3 V_n} \Delta r + \Delta \dot{V} - \frac{KM \dot{r}_n}{V_n^2 r_n^2} \Delta V = -\frac{\Delta D}{m} \quad (3.9)$$

The lift and drag forces are defined in the following way

$$L = \frac{1}{2} \cdot \frac{AV^2 \rho C_L}{m} \quad (3.10)$$

$$D = \frac{1}{2} \cdot \frac{AV^2 \rho C_D}{m} \quad (3.11)$$

where  $C_L$  and  $C_D$  are lift and drag coefficients, respectively. The density is defined by equation (2.19)

$$\rho = \rho_0 e^{-\beta h} \quad (3.12)$$

As the reentry vehicle is a constant trim lifting vehicle the  $C_L$  and  $C_D$  will remain constant during the flight. Substituting equations (3.7) and

$$h = h_n + \Delta h \quad (3.13)$$

into equations (3.10) and (3.11) gives the deviations of  $L$  and  $D$

$$\Delta L = \frac{2L_n}{V_n} \Delta V - \beta L_n \Delta h + \Delta F_z \quad (3.14)$$

$$\Delta D = \frac{2D_n}{V_n} \Delta V - \beta D_n \Delta h - \Delta F_x \quad (3.15)$$

To equations (3.14) and (3.15) have been added  $\Delta F_x$  and  $\Delta F_z$  which represent additional forces along nominal  $L$  and  $V$  directions. They may be forces, caused by the control system, to correct the flight path. The choice of subscripts will be obvious in the next section.

Substituting equations (3.14) and (3.15) into equations (3.8) and (3.9), respectively, and remembering that  $\Delta r = \Delta h$ , gives the perturbation equations in the following form

$$\begin{aligned} \Delta \ddot{r} - \frac{\dot{V}_n}{V_n} \Delta \dot{r} + \left( \frac{V_n^2}{r_n^2} - \frac{2KM}{r_n^3} + \frac{\beta L_n}{m} \right) \Delta r - \frac{\dot{r}_n}{V_n} \Delta \dot{V} + \\ + \left( \frac{\dot{r}_n \dot{V}_n}{V_n^2} - \frac{2V_n}{r_n} - \frac{2L_n}{V_n m} \right) \Delta V = \frac{\Delta F_z}{m} \end{aligned} \quad (3.16)$$

$$\begin{aligned} \frac{KM}{r_n^2 V_n} \Delta \dot{r} - \left( \frac{2KM \dot{r}_n}{r_n^3 V_n} + \frac{\beta D_n}{m} \right) \Delta r + \Delta \dot{V} + \\ - \left( \frac{KM \dot{r}_n}{V_n^2 r_n^2} - \frac{2D_n}{V_n m} \right) \Delta V = \frac{\Delta F_x}{m} \end{aligned} \quad (3.17)$$

Treating the coefficients of equations (3.16) and (3.17) as constants, the two equations can be solved simultaneously. The characteristics of the nominal trajectory have been calculated earlier in section 2.4 and are now substituted into the coefficients of equations (3.16) and (3.17) together with  $KM/r_n^2 = g$ . Several terms in the coefficients are very small and can be neglected compared to others. If this is done, the simplified solutions come out as follows:

$$\begin{aligned} \Delta \ddot{r} + \frac{g(1 - \bar{V}_n^2)}{V_s \bar{V}_n (\frac{L}{D})_n} \Delta \ddot{r} + \beta g(1 - \bar{V}_n^2) \Delta \dot{r} = \frac{\Delta \dot{F}_z}{m} + \frac{2g}{V_s (\frac{L}{D})_n} \cdot \\ \cdot \frac{1 - \bar{V}_n^2}{\bar{V}_n} \frac{\Delta F_z}{m} - \frac{2}{r \beta (\frac{L}{D})_n \bar{V}_n^2} \cdot \frac{\Delta \dot{F}_x}{m} + \\ + \frac{2V_s}{r \bar{V}_n} \cdot \frac{\Delta F_x}{m} \end{aligned} \quad (3.18)$$



$$\begin{aligned}
\Delta\ddot{V} + \frac{g(1 - \bar{V}_n^2)}{V_s \bar{V}_n \left(\frac{L}{D}\right)_n} \Delta\dot{V} + \beta g(1 - \bar{V}_n^2) \Delta\dot{V} &= \frac{\Delta F_x}{m} + \\
+ \frac{g(1 - \bar{V}_n^2)}{V_s \bar{V}_n \left(\frac{L}{D}\right)_n} \cdot \frac{\Delta \dot{F}_x}{m} + \beta g(1 - \bar{V}_n^2) \cdot \frac{\Delta F_x}{m} + \\
+ \frac{2}{\bar{V}_n^2 r \beta \left(\frac{L}{D}\right)_n} \cdot \frac{\Delta \ddot{F}_z}{m} - \frac{g}{\bar{V}_n V_s} \cdot \frac{\Delta \dot{F}_z}{m} + \\
+ \frac{\beta g}{\left(\frac{L}{D}\right)_n} (1 - \bar{V}_n^2) \frac{\Delta F_z}{m}
\end{aligned} \tag{3.19}$$

The coefficients that are most important when deriving equations (3.18) and (3.19) are those connected to the altitude or density change.

By using Laplace transform technique on equations (3.18) and (3.19)

these equations are transformed into

$$\begin{aligned}
s \left[ s^2 + \frac{g(1 - \bar{V}_n^2)}{V_s \bar{V}_n \left(\frac{L}{D}\right)_n} s + \beta g(1 - \bar{V}_n^2) \right] \Delta r &= \left[ s + \frac{2g}{V_s \left(\frac{L}{D}\right)_n} \cdot \frac{1 - \bar{V}_n^2}{\bar{V}_n} \right] \cdot \frac{\Delta F_z}{m} - \\
- \frac{2}{r \beta \bar{V}_n^2 \left(\frac{L}{D}\right)_n} \left[ s - V_s \beta \left(\frac{L}{D}\right)_n \bar{V}_n \right] \frac{\Delta F_x}{m}
\end{aligned} \tag{3.20}$$

$$\begin{aligned}
s \left[ s^2 + \frac{g(1 - \bar{V}_n^2)}{V_s \bar{V}_n \left(\frac{L}{D}\right)_n} s + \beta g(1 - \bar{V}_n^2) \right] \Delta V &= \left[ s^2 + \frac{g(1 - \bar{V}_n^2)}{V_s \bar{V}_n \left(\frac{L}{D}\right)_n} \cdot s + \right. \\
+ \beta g(1 - \bar{V}_n^2) \left. \right] \frac{\Delta F_x}{m} + \frac{2}{r \beta \bar{V}_n^2 \left(\frac{L}{D}\right)_n} \left[ s^2 - \frac{1}{2} \beta V_s \bar{V}_n \left(\frac{L}{D}\right)_n s + \right. \\
+ \left. \frac{1}{2} r g \beta^2 \bar{V}_n^2 (1 - \bar{V}_n^2) \right] \frac{\Delta F_z}{m}
\end{aligned} \tag{3.21}$$

The natural frequency,  $\omega_n$ , and relative damping,  $\zeta$ , at local points along the equilibrium glide trajectory are:

Natural frequency

$$\omega_n^2 = \beta g (1 - \bar{V}_n^2) \quad (3.22)$$

Relative damping

$$\zeta = \frac{1}{2\sqrt{\beta r} \left(\frac{L}{D}\right)_n} \cdot \frac{\sqrt{1 - \bar{V}_n^2}}{\bar{V}_n} \quad (3.23)$$

It is seen from equation (3.22) and (3.23) that the spring constant  $\omega_n^2$  is positive and  $\zeta > 0$ , thus, the system is stable. The natural frequency is increasing with decreasing dimensionless velocity  $\bar{V}$ . The damping is very small and increasing with decreasing velocity, but, always less than 0.05 for  $\bar{V}_n > 0.2$  and  $L/D = 0.5$ . Thus, the damping can be neglected in most applications. To make the handling of equations (3.20) and (3.21) easier the following notations are introduced

$$\Delta r = G_1(s) \cdot \Delta F_z + G_2(s) \cdot \Delta F_x \quad (3.24)$$

$$\Delta V = G_3(s) \cdot \Delta F_z + G_4(s) \cdot \Delta F_x \quad (3.25)$$

where

$$G_1(s) = \frac{1}{m} \cdot \frac{\left[ s + \frac{2g}{V_s \left(\frac{L}{D}\right)_n} \cdot \frac{1 - \bar{V}_n^2}{\bar{V}_n} \right]}{s \left[ s^2 + \frac{g(1 - \bar{V}_n^2)}{V_s \bar{V}_n \left(\frac{L}{D}\right)_n} s + \beta g (1 - \bar{V}_n^2) \right]} \quad (3.26)$$

and

$$G_2(s) = \frac{-2}{m \cdot r \beta \bar{V}_n^2 \left(\frac{L}{D}\right)_n} \cdot \frac{\left[ s - V_s \beta \left(\frac{L}{D}\right)_n \bar{V}_n \right]}{s \left[ s^2 + \frac{g(1 - \bar{V}_n^2)}{V_s \bar{V}_n \left(\frac{L}{D}\right)_n} s + \beta g(1 - \bar{V}_n^2) \right]} \quad (3.27)$$

$$G_3(s) = \frac{2}{m \cdot r \beta \bar{V}_n^2 \left(\frac{L}{D}\right)_n} \cdot \frac{\left[ s^2 - \frac{1}{2} \beta V_s \bar{V}_n \left(\frac{L}{D}\right)_n s + \frac{1}{2} r g \beta^2 \bar{V}_n^2 (1 - \bar{V}_n^2) \right]}{s \left[ s^2 + \frac{g(1 - \bar{V}_n^2)}{V_s \bar{V}_n \left(\frac{L}{D}\right)_n} s + \beta g(1 - \bar{V}_n^2) \right]} \quad (3.28)$$

$$G_4(s) = \frac{1}{m} \cdot \frac{1}{s} \quad (3.29)$$

### 3.3 The Vehicle Transfer Functions

Equation (2.18) shows that the range to go for the vehicle is proportional to  $L/D$ , or perhaps, more specific  $(L/D)_V$  which is the vertical component of  $L/D$ . By controlling the vertical component of the ratio lift-to-drag, it is thus possible to control the range of the vehicle. The control of  $(L/D)_V$  can be done by rolling the vehicle to an angle so that the lift vector points out from the vertical plane. Variation of the roll angle will then increase or decrease the ratio  $(L/D)_V$ .

When the vehicle is oscillating about the nominal flight path the velocity vector  $\vec{V}$  will tilt a small angle,  $\bar{\epsilon}$ , from the nominal velocity vector  $\vec{V}_n$ . This tilts, also, the lift and drag vector introducing further forces besides those earlier studied along the  $L_n$  and  $V_n$  directions. The ordinary control

forces are coming from small changes of the roll angle and those forces will keep the vehicle close to the nominal trajectory.

If the tilting of the velocity vector about the nominal direction is small, it may be possible to neglect the additional forces it introduces. The following calculations will give the answer to that question and present the transfer functions of the vehicle from roll angle changes to the variables describing the motion of the vehicle.

The nominal flight path defines a coordinate system  $xyz$  in such a way that  $x$  falls along  $\vec{V}_n$  and the  $xz$ -plane lies in the vertical plane. See Fig. 3.1.

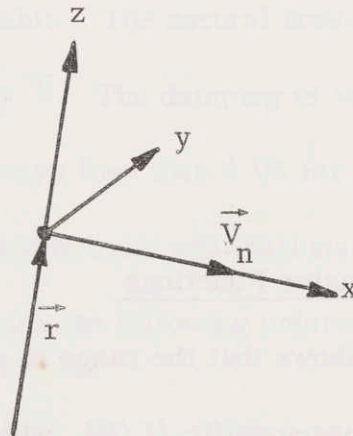


Fig. 3.1 The  $xyz$ -Coordinate System

Another coordinate system  $XYZ$  is defined by the actual velocity  $\vec{V}$  and lift force  $\vec{L}$  as indicated in Fig. 3.2. The relations between the two coordinate systems can be derived in two steps. An intermediate coordinate system is rotated from the  $xyz$ -system the small angle  $\bar{\epsilon}$ , which has the components  $0, \epsilon_y, \epsilon_z$ . The relations between the intermediate coordinate system, here called  $X_1Y_1Z_1$ , and the original  $xyz$ -system are as follows, if the small angle assumption is applied.

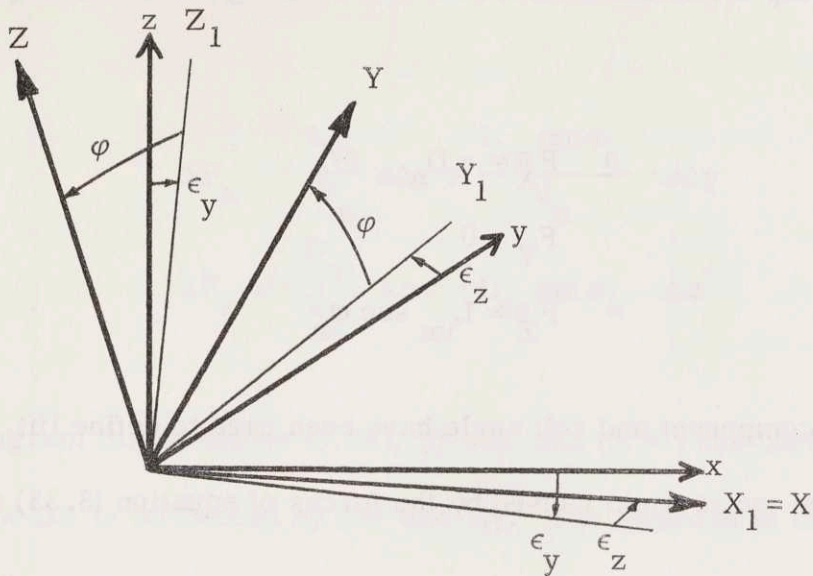


Fig. 3.2 The Coordinate Systems XYZ and xyz.

$$\begin{bmatrix} X_1 \\ Y_1 \\ Z_1 \end{bmatrix} = \begin{bmatrix} 1 & \epsilon_z & -\epsilon_y \\ -\epsilon_z & 1 & 0 \\ \epsilon_y & 0 & 1 \end{bmatrix} \begin{bmatrix} x \\ y \\ z \end{bmatrix} \quad (3.30)$$

The intermediate coordinate system is related to the XYZ-system by a rotation  $\varphi$  about the  $X_1$ -axis. Transformations between the  $X_1Y_1Z_1$ -system and the XYZ-system are described by

$$\begin{bmatrix} X \\ Y \\ Z \end{bmatrix} = \begin{bmatrix} 1 & 0 & 0 \\ 0 & \cos \varphi & \sin \varphi \\ 0 & -\sin \varphi & \cos \varphi \end{bmatrix} \begin{bmatrix} X_1 \\ Y_1 \\ Z_1 \end{bmatrix} \quad (3.31)$$

The relation between the XYZ-system and the xyz-system can be solved from equations (3.30) and (3.31). The result is

$$\begin{bmatrix} x \\ y \\ z \end{bmatrix} = \begin{bmatrix} 1 & (-\epsilon_z \cos \varphi + \epsilon_y \sin \varphi) & (\epsilon_z \sin \varphi + \epsilon_y \cos \varphi) \\ \epsilon_z & \cos \varphi & -\sin \varphi \\ -\epsilon_y & \sin \varphi & \cos \varphi \end{bmatrix} \begin{bmatrix} X \\ Y \\ Z \end{bmatrix} \quad (3.32)$$

Introducing the nominal values for lift and drag in the XYZ-system

yields

$$\begin{aligned} F_X &= -D_n \\ F_Y &= 0 \\ F_Z &= L_{vn} \sec \varphi_n \end{aligned} \quad (3.33)$$

where vertical component and roll angle have been used to define lift. The forces

$F_x, F_y, F_z$  in the xyz-system caused by the forces of equation (3.33) are

$$\begin{aligned} F_x &= -D_n + L_{vn} \sec \varphi_n (\epsilon_z \sin \varphi + \epsilon_y \cos \varphi) \\ F_y &= -D_n \epsilon_z - L_{vn} \sec \varphi_n \sin \varphi \\ F_z &= D_n \epsilon_y + L_{vn} \sec \varphi_n \cos \varphi \end{aligned} \quad (3.34)$$

The effect of small variations of  $\epsilon$  and  $\varphi$  can be found by differentiation of equation (3.34). If the partial derivatives are calculated for  $\epsilon_y = \epsilon_z = 0$  and  $\varphi = \varphi_n$ , the differentiation gives

$$\Delta F_x = L_{vn} \Delta \epsilon_y + L_{vn} \tan \varphi_n \Delta \epsilon_z \quad (3.35)$$

$$\Delta F_y = -D_n \Delta \epsilon_z - L_{vn} \Delta \varphi \quad (3.36)$$

$$\Delta F_z = D_n \Delta \epsilon_y - L_{vn} \tan \varphi_n \Delta \varphi \quad (3.37)$$

The  $\epsilon$ -angles depend upon the velocities in y and z directions

$$\Delta \epsilon_y = -\frac{s \Delta r}{V_n} \quad (3.38)$$

$$\Delta \epsilon_z = \frac{s \Delta y}{V_n} \quad (3.39)$$

The force differences  $\Delta F_x$  and  $\Delta F_z$  correspond to the differences of equations

(3.24) and (3.25). Substituting equations (3.38) and (3.39) into (3.35) and (3.37)

gives

$$\Delta F_x = -\frac{L_{vn}}{V_n} s\Delta r + \frac{L_{vn} \tan \varphi_n}{V_n} \cdot s\Delta y \quad (3.40)$$

$$\Delta F_z = -\frac{D_n}{V_n} \cdot s\Delta r - L_{vn} \tan \varphi_n \cdot \Delta \varphi \quad (3.41)$$

A block diagram for equations (3.24), (3.40), and (3.41) has been drawn in Fig. 3.3 to show how  $\Delta r$  is influenced by  $\Delta \varphi$  and  $\Delta y$ . The feedback in the upper half of the figure can be neglected as

$$\left| s \cdot \frac{L_{vn}}{V_n} G_2 \right|_{s=j\omega} \ll 1 \quad (3.42)$$

and the block diagram is redrawn in Fig. 3.4. The transfer function from  $\Delta \varphi$  to  $\Delta r$  is

$$\frac{\Delta r}{\Delta \varphi} = -L_{vn} \tan \varphi_n \frac{G_1}{1 + s \cdot \frac{D_n}{V_n} G_1} \quad (3.43)$$

Substituting equations (2.39), (2.40), and (3.26) into equation (3.43) gives the following transfer function

$$\frac{\Delta r}{\Delta \varphi} = -g(1-\bar{V}^2) \tan \varphi_n \cdot \frac{\left[ s + \frac{2g}{V_s \left(\frac{L}{D}\right)_{vn}} \cdot \frac{1-\bar{V}_n^2}{\bar{V}_n} \right]}{s \left[ s^2 + \frac{2g}{V_s \left(\frac{L}{D}\right)_{vn}} \cdot \frac{1-\bar{V}_n^2}{\bar{V}_n} s + \beta g(1-\bar{V}_n^2) \left( 1 + \frac{2g}{\beta V_s^2 \left(\frac{L}{D}\right)_{vn}^2} \cdot \frac{1-\bar{V}_n^2}{\bar{V}_n^2} \right) \right]} \quad (3.44)$$

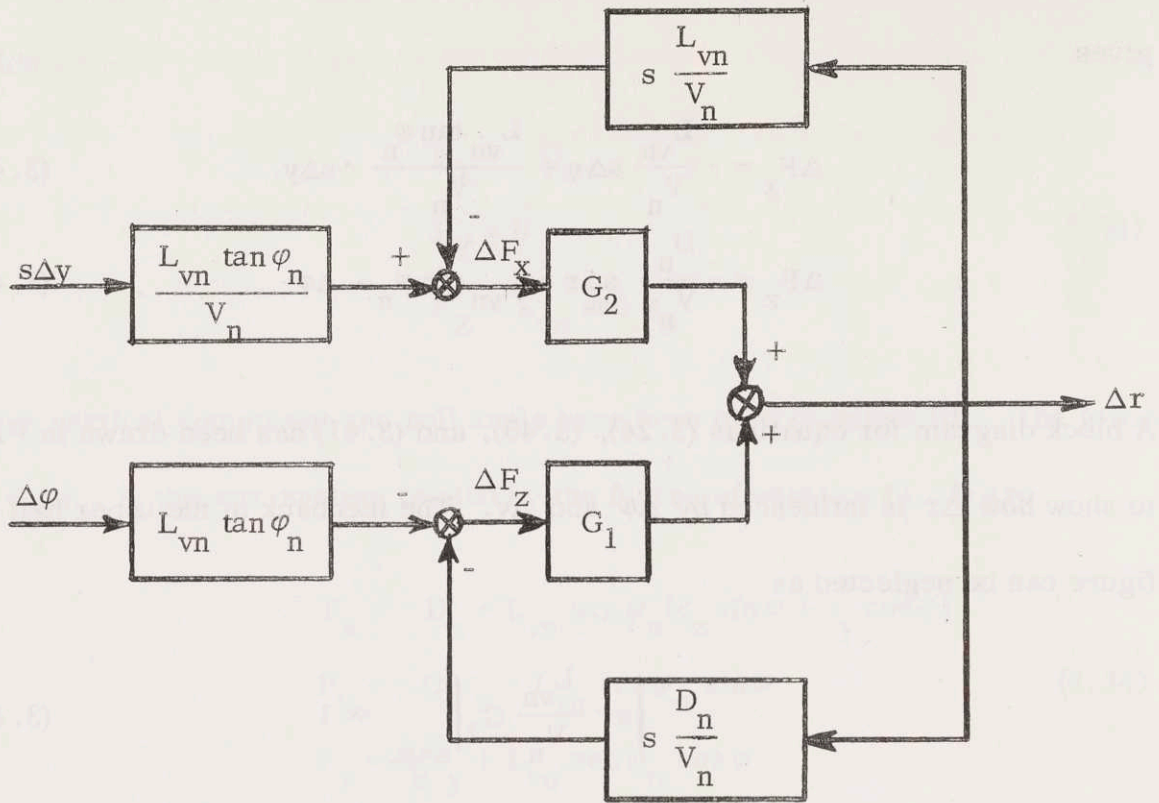


Fig. 3.3 Block Diagram for  $\Delta r$ .

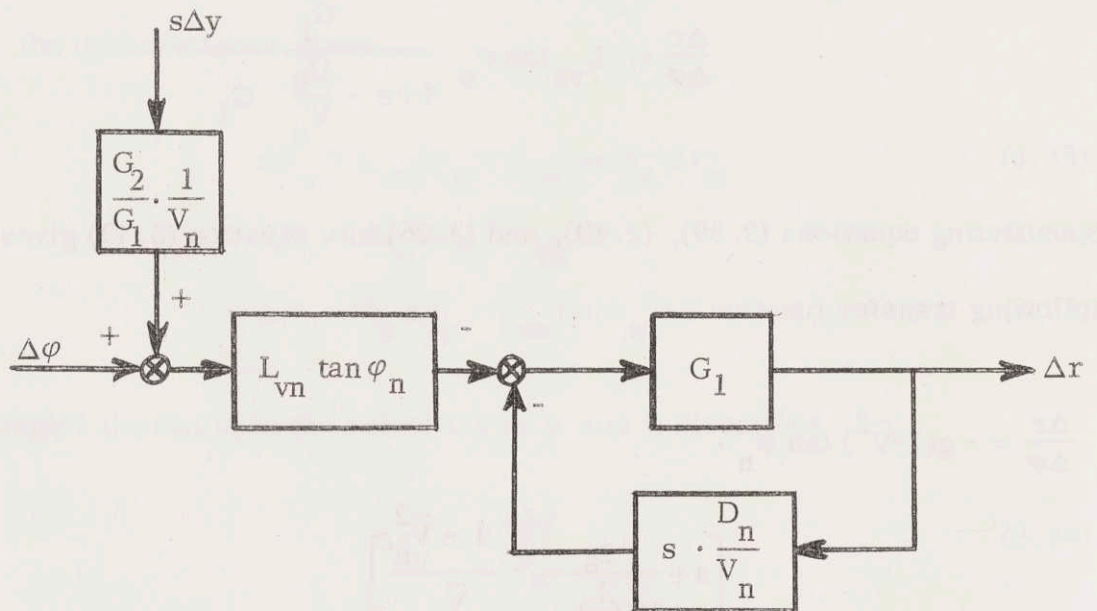


Fig. 3.4 Simplified  $\Delta r$ -Block Diagram.



Here  $(L/D)$  of Chapter 2 has been used as  $(L/D)_v$  as the lift vector is rolled to an angle. The damping of equation (3.44) is twice as much as that one of equation (3.26) but is still very small. The natural frequency of equation (3.44) has increased compared to the natural frequency of equation (3.26) but the increase is less than 11% for  $\bar{V}_n > 0.2$  and  $(L/D)_{vn} = 0.5$ . Equation (3.44) may therefore be approximated to

$$\frac{\Delta r}{\Delta \phi} \approx -g(1 - \bar{V}_n^2) \tan \phi_n \frac{\left[ s + \frac{2g}{V_s \left(\frac{L}{D}\right)_{vn}} \cdot \frac{1 - \bar{V}_n^2}{\bar{V}_n} \right]}{s \left[ s^2 + \beta g(1 - \bar{V}_n^2) \right]} \quad (3.45)$$

In a similar way, as above, a block diagram for  $\Delta V$  can be drawn starting from equation (3.25) and also using equations (3.40), (3.41) and (3.45). The resulting block diagram is shown in Fig. 3.5. Analyzing the paths from  $\Delta \phi$  to  $\Delta V$  it is found that the upper path

$$\Delta V = -L_{vn} \tan \phi_n \cdot G_3 \Delta \phi \quad (3.46)$$

is the dominating one except for the resonance frequency of  $\Delta r/\Delta \phi$ . It is therefore possible to redraw the block diagram as shown in Fig. 3.6. Substituting equations (2.40) and (3.28) into equation (3.46) gives the transfer function from  $\Delta \phi$  to  $\Delta V$ .

$$\frac{\Delta V}{\Delta \phi} = -\frac{2g \tan \phi_n}{r\beta(L/D)_{vn}} \cdot \frac{1 - \bar{V}_n^2}{\bar{V}_n^2} \cdot \frac{\left[ s^2 - \frac{1}{2} \frac{V_s \bar{V}_n \left(\frac{L}{D}\right)_{vn}}{r} s + \frac{1}{2} r g \frac{2 - \bar{V}_n^2(1 - \bar{V}_n^2)}{\bar{V}_n^2} \right]}{s \left[ s^2 + \frac{g}{V_s \left(\frac{L}{D}\right)_{vn}} \cdot \frac{1 - \bar{V}_n^2}{\bar{V}_n} s + \beta g(1 - \bar{V}_n^2) \right]} \quad (3.47)$$

A similar approximation as above can be applied to equation (3.47) for the interesting frequency range,  $\omega < 5$  rad/sec.

$$\frac{\Delta V}{\Delta \varphi} \approx - \frac{g^2 \beta \tan \varphi_n}{(L/D)_{vn}} \cdot (1 - \bar{V}_n^2)^2 \cdot \frac{1}{s \left[ s^2 + \beta g (1 - \bar{V}_n^2) \right]} \quad (3.47)$$

The influence of  $s\Delta y$  will not be treated here.

When designing the range control, transfer functions from  $(L/D)_v$  to  $\Delta r$  and  $\Delta V$  will be useful. The  $(L/D)_v$  as controlled by the roll angle is given by

$$\left( \frac{L}{D} \right)_v = \frac{1}{D_n} \cdot \frac{L_{vn}}{\cos \varphi_n} \cos \varphi \quad (3.49)$$

Differentiation of equation (3.49)

$$\Delta \left( \frac{L}{D} \right)_v = - \left( \frac{L}{D} \right)_{vn} \tan \varphi_n \cdot \Delta \varphi \quad (3.50)$$

Substituting equation (3.50) into (3.45) and (3.48) yields

$$\frac{\Delta r}{\Delta \left( \frac{L}{D} \right)_v} = \frac{g(1 - \bar{V}_n^2)}{(L/D)_{vn}} \cdot \frac{\left[ s + \frac{2g}{V_n \left( \frac{L}{D} \right)_{vn}} \cdot \frac{1 - \bar{V}_n^2}{\bar{V}_n} \right]}{s \left[ s^2 + \beta g (1 - \bar{V}_n^2) \right]} \quad (3.51)$$

and

$$\frac{\Delta V}{\Delta \left( \frac{L}{D} \right)_v} = \frac{g^2 \beta (1 - \bar{V}_n^2)^2}{(L/D)_{vn}^2} \cdot \frac{1}{s \left[ s^2 + \beta g (1 - \bar{V}_n^2) \right]} \quad (3.52)$$

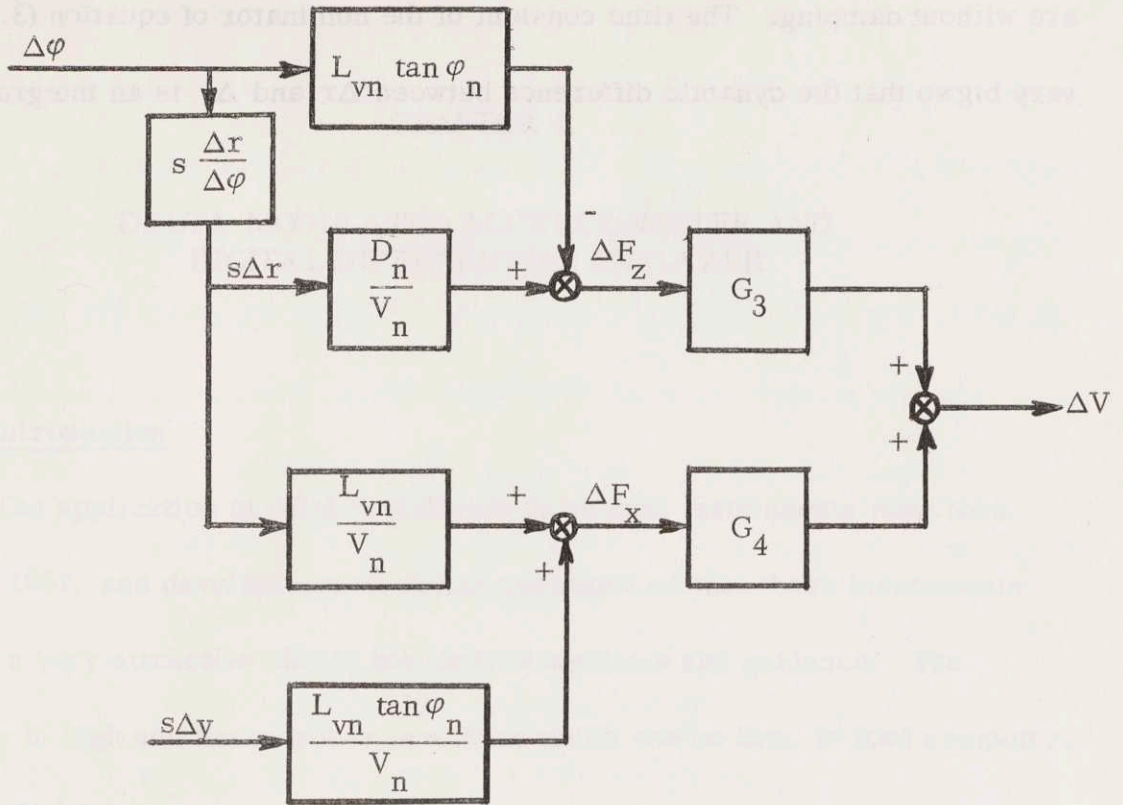


Fig. 3.5 Block Diagram for  $\Delta V$ .

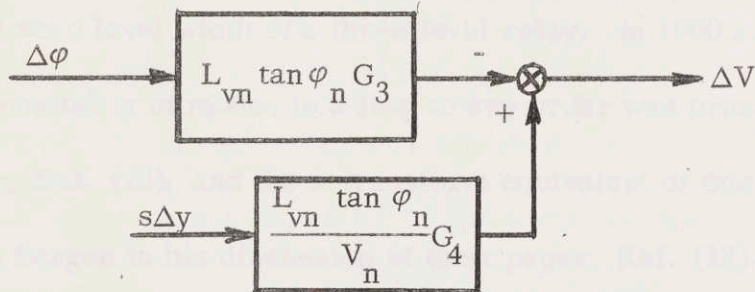


Fig. 3.6 Simplified  $\Delta V$ -Block Diagram.

These equations describe the long period motion of the vehicle. Both functions are without damping. The time constant of the nominator of equation (3.51) is very big so that the dynamic difference between  $\Delta r$  and  $\Delta v$  is an integration.

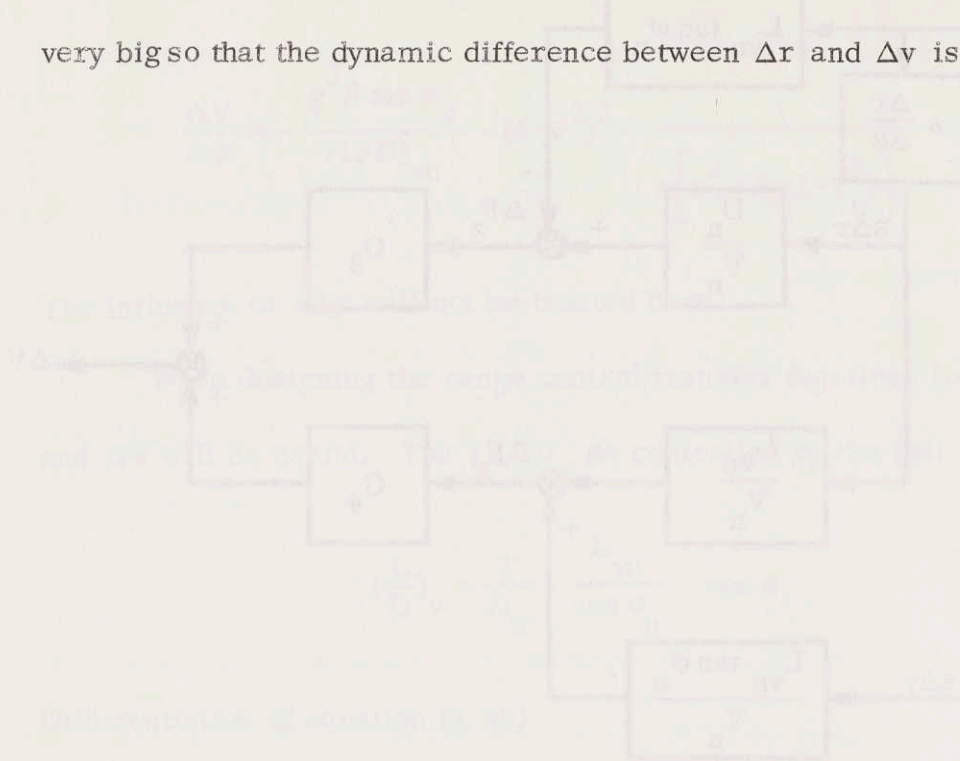


Fig. 3.5 Block Diagram for  $\Delta r$

(3.50)



Fig. 3.6 Simplified  $\Delta r$  Block Diagram

(3.51)

(3.52)

## CHAPTER 4

### DELTA-MODULATED ACCELEROMETER AND DIGITAL DIFFERENTIAL ANALYZER

#### 4.1 Introduction

The application of delta modulation to inertial instruments first took place in 1957, and development work has continued so that these instruments are now a very attractive choice for inertial systems and guidance. The accuracy is high and the output is in a form which can be used to feed computers of the digital type.

Most of the theoretical attention has been paid to the zero-input behaviour of delta modulated loops. Several authors, i. e., Ref. (17), used the phase plane method in their studies and an extended describing function was used by Chow, Ref. (14), to eliminate limit cycles in delta modulated loops by adjusting the zero level width of a three level relay. In 1960 an exact method for testing the possibility of modes in a loop of any order was presented by Torng and Meserve, Ref. (12), and the z-transform equivalent of this method was suggested by Bergen in his discussion of their paper, Ref. (13). Wiener has applied their method on delta modulated accelerometers, Ref. (3).

This thesis is concerned with the question, if the delta modulated accelerometer will cause a limit cycle in the range control loop. Therefore a non-linear model of the delta modulated accelerometer for sinusoid inputs will

be derived in this chapter.

The overall mission of a space vehicle would require a general purpose digital computer, but in this thesis the reentry control is treated as a special problem and a DDA-computer will be used for the control calculations. The DDA has been described as a computer with the speed of an analog computer and the accuracy of a digital computer. It has the advantage of not requiring time to be the independent variable of integration. The DDA is described in the literature, Ref. (4), (5), and (6), and only a very short review will be given in this chapter.

## 4.2 Delta-Modulated Loops

### 4.2.1 Description of the Loop

Delta modulated loops are shown in Fig. 4.1 and 4.2 with a two level and a three level relay, respectively. The input is translated into a sequence of pulses, each having the same value, but with either polarity being possible. One of the linear plants may be unity. When the loop is used for transmission, the linear plant in the forward path is usually unity, while in instrumentation applications the feedback plant usually contains a zero-order hold. Usually there is an integration in the loop to assure zero average error. The mathematical model for the sampler is an impulse modulator synchronized with a clock. Each impulse appearing at the output represents a unit change in the input or one of its integrals or derivatives. This representation of a signal in terms of increments leads to the name "delta modulation." If the integration appears in the forward path, each output pulse represents a change in the integral of the input. If the integration appears in the feedback path, each pulse represents a change in the input itself.

Without input, a loop with a two-level relay will experience self-excited oscillation at half cycle, and if the zero level is narrow enough,

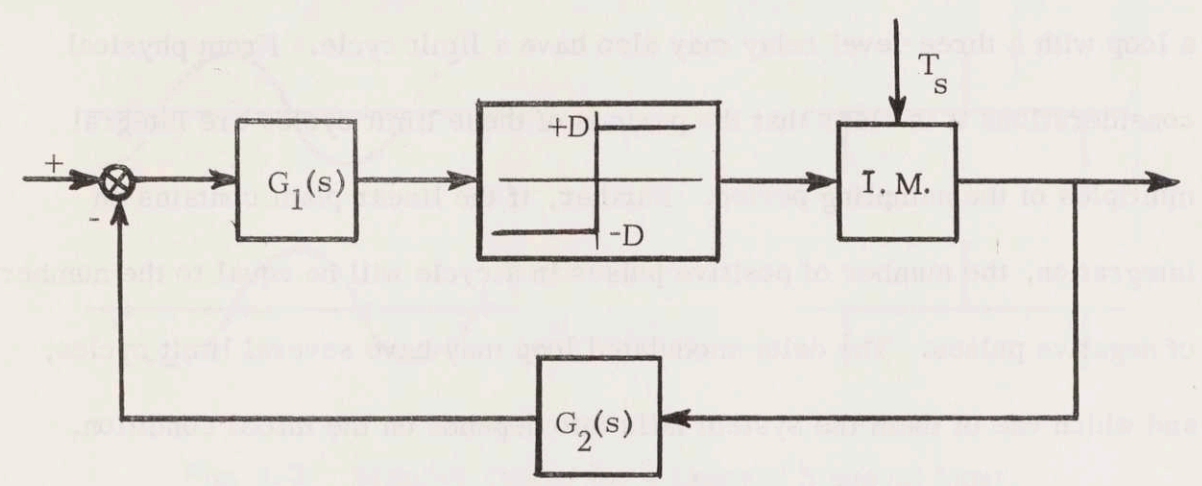


Fig. 4.1 Delta-Modulated Loop with Two Level Relay.

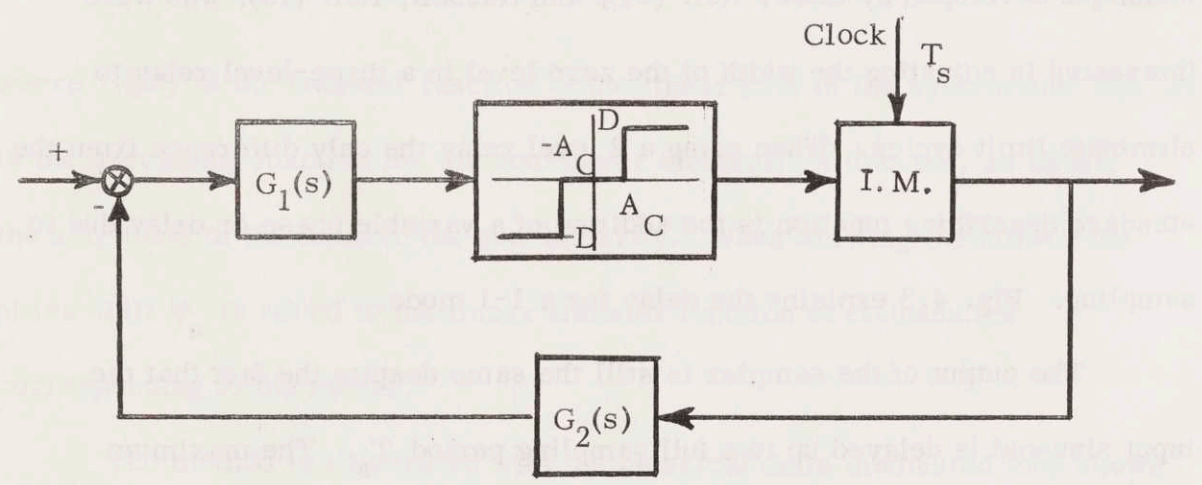


Fig. 4.2 Delta-Modulated Loop with Three Level Relay.

#### 4.2.2 Describing Function Analysis

Without input, a loop with a two-level relay will experience self-excited oscillation or limit cycle, and if the zero level is narrow enough, a loop with a three-level relay may also have a limit cycle. From physical considerations it is clear that the periods of these limit cycles are integral multiples of the sampling period. Further, if the linear plant contains an integration, the number of positive pulses in a cycle will be equal to the number of negative pulses. The delta-modulated loop may have several limit cycles, and which one of them the system falls into depends on the initial condition. Each limit cycle is characterized by the sequence of output pulses and are usually referred to as a certain mode. A sequence of one positive pulse followed by a negative pulse is called a 1-1 mode. Similarly two positive pulses followed by two negative is called a 2-2 mode. An approximate idea of the possible modes can be obtained by using an extended version of the describing function technique developed by Chow, Ref. (14), and Russell, Ref. (15), who were interested in adjusting the width of the zero level in a three-level relay to eliminate limit cycles. When using a 2 level relay the only difference from the standard describing function is the addition of a variable phase or delay due to sampling. Fig. 4.3 explains the delay for a 1-1 mode.

The output of the sampler is still the same despite the fact that the input sinusoid is delayed up to a full sampling period  $T_s$ . The maximum phase shift due to sampling,  $\phi_n$ , for the different modes is given by

$$\phi_n = \omega_n T_s = \frac{\pi}{n} \quad (4.1)$$

The notation  $n$  stands for the number of the mode, thus  $n=1$  means mode 1-1



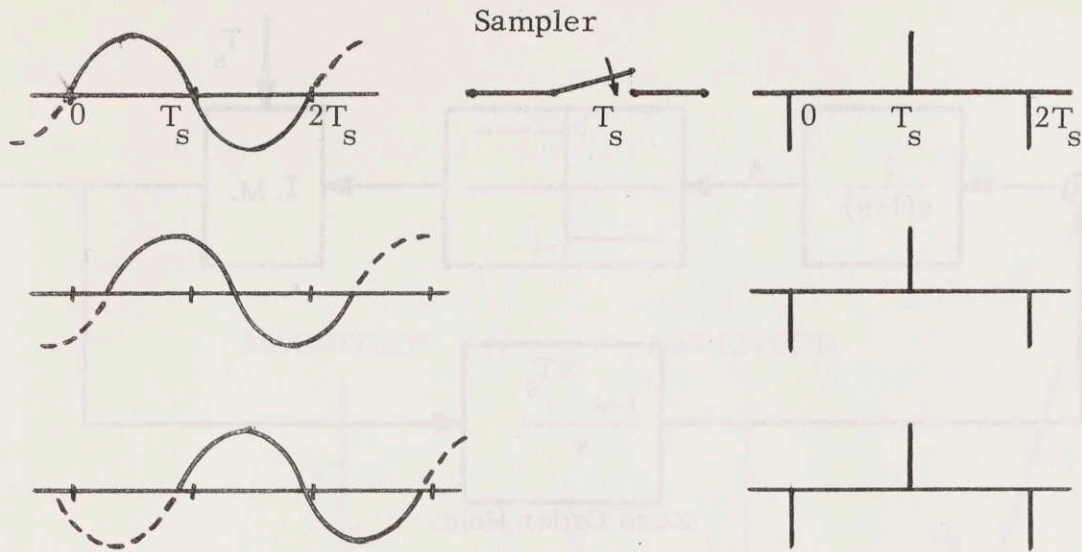


Fig. 4.3 Sampler Output for a Delayed Sinusoid Input.

and  $\omega_1$  is the frequency of the same mode.

The describing function analysis is carried out by graphical solution of the equation

$$1 + G(j\omega)N(A, \omega) = 0 \quad (4.2)$$

where  $G(j\omega)$  is the transfer function of the linear part of the system and  $N(A, \omega)$  is the describing function for the non-linear element.  $A$  denotes, as usual, the amplitude of the input to the non-linearity. When drawing the curves the phase shift  $\phi_n$  is added to the linear transfer function at frequencies corresponding to the modes.

The method is illustrated with the classical delta modulated loop shown in Fig. 4.4. The "moding plot" of the delta-modulated loop in Fig. 4.4 is drawn in Fig. 4.5 and indicates that 1-1, 2-2 and 3-3 modes are possible. If any of the modes have to be eliminated, the frequency curve of Fig. 4.4 must

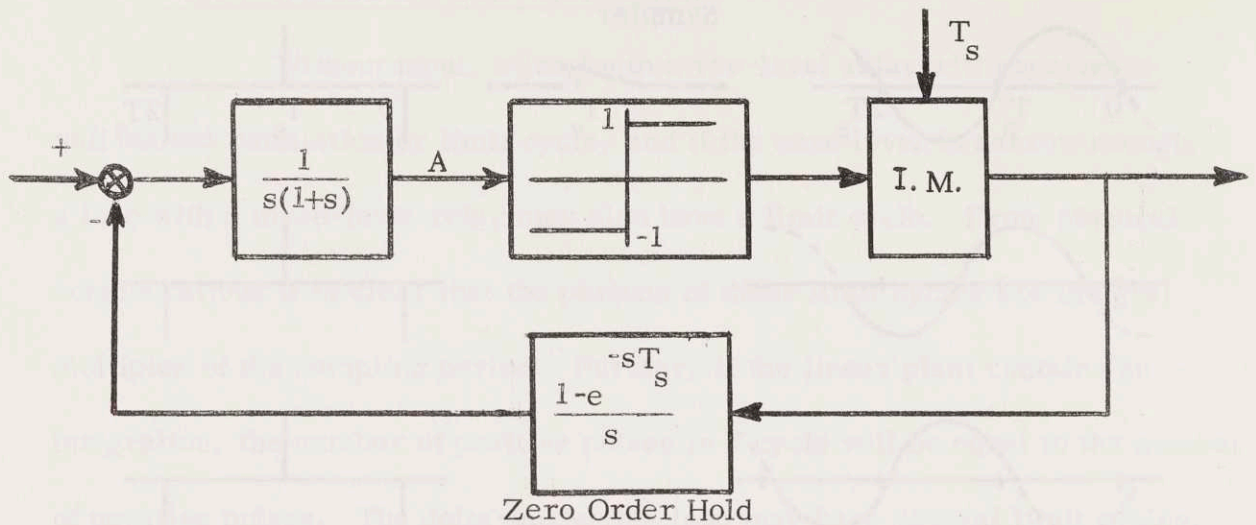


Fig. 4.4 A Delta-Modulated Loop.

be moved to the right by using compensation. However, there exists a second alternative when eliminating modes. The two-level relay can be exchanged for a three-level relay whose describing function has a maximum and  $N^{-1}$  in Fig. 4.5 thus gets a minimum. If  $N^{-1}$  has its minimum above the 3-3 mode, the system will not experience a limit cycle. The added phase lags are for the three-level relay case only approximate but give a good idea of the behaviour of the loop.

#### 4.3 Delta-Modulated Accelerometer

The accelerometer, when behaving in an ideal manner, is described by the following differential equation

$$J\ddot{A}_{OA} + C\dot{A}_{OA} = Pa_{IA} + M_{tg} \quad (4.3)$$

where the symbols are

- J      moment of inertia about output axis
- C      damping coefficient of fluid damper

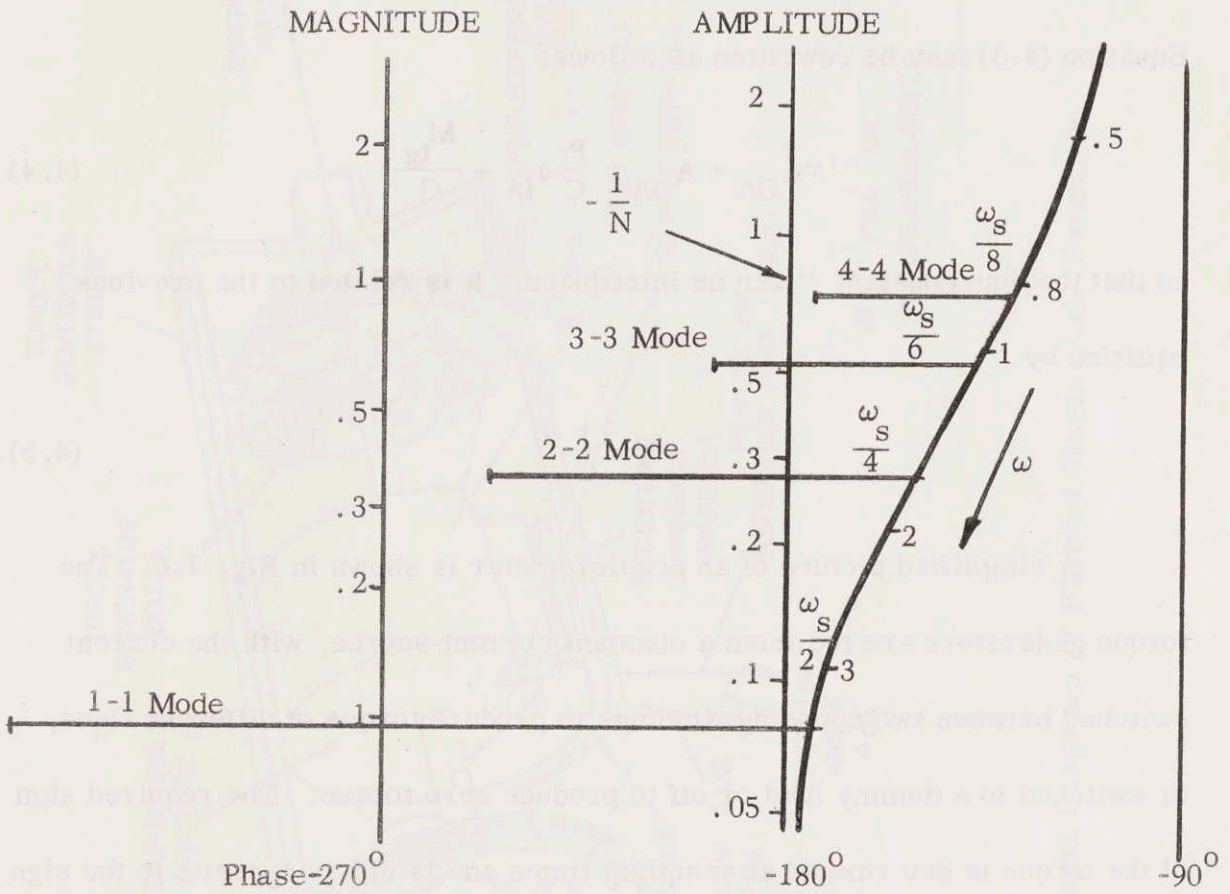


Fig. 4.5 Moding Plot.

P	pendulosity of accelerometer
$M_{tg}$	torque applied to the instrument float by the torque generator
$A_{OA}$	angle through which the float has turned with respect to the case about the instrument output axis
$a_{IA}$	non-gravitational acceleration of the instrument with respect to inertial space along the input axis.

Equation (4.3) may be rewritten as follows:

$$\tau \ddot{A}_{OA} + \dot{A}_{OA} = \frac{P}{C} a_{IA} + \frac{M_{tg}}{C} \quad (4.4)$$

so that the time constant  $\tau$  can be introduced. It is related to the previous equation by

$$\tau = \frac{J}{C} \quad (4.5)$$

A simplified picture of an accelerometer is shown in Fig. 4.6. The torque generators are fed from a constant current source, with the current switched between two opposing windings to produce torque of different signs, or switched to a dummy load or off to produce zero torque. The required sign of the torque is determined at sampling times and is either opposite to the sign of the float angle or zero depending on the logic of the loop. Therefore, the torque generator acts as a zero-order hold in the feedback path. A block-diagram of the delta-modulated accelerometer takes the form shown in Fig. 4.7. The new symbol M stands for the torque level of the torque generator.

In this investigation the parameters for a non-limit cycling accelerometer will be derived and the following calculations will show how the limit cycles can be removed by using a three level relay. A limit cycling accelerometer often introduces error in the following guidance computer calculations as

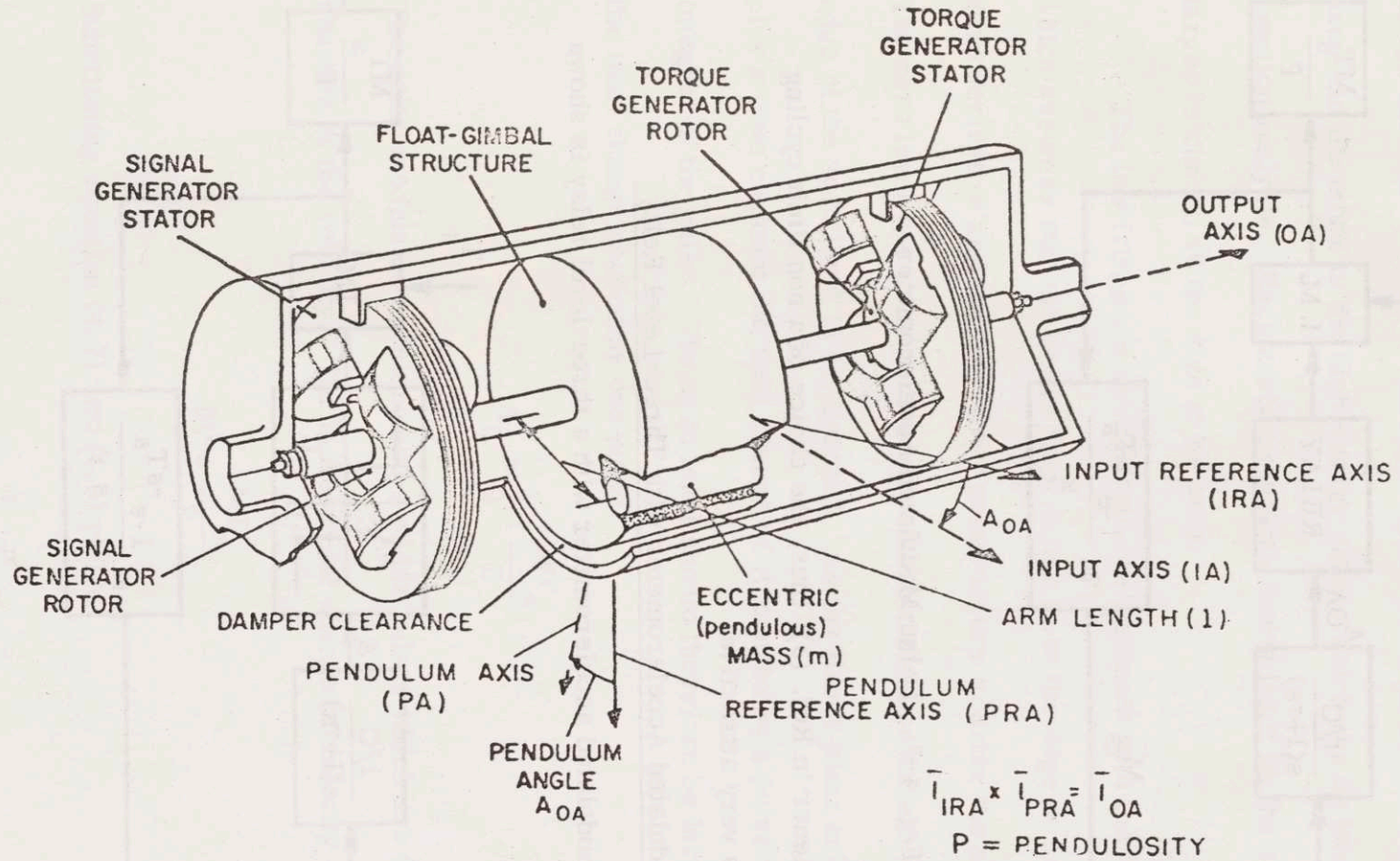


Fig. 4.6 Pictorial Diagram of Floated Single-Axis Pendulum

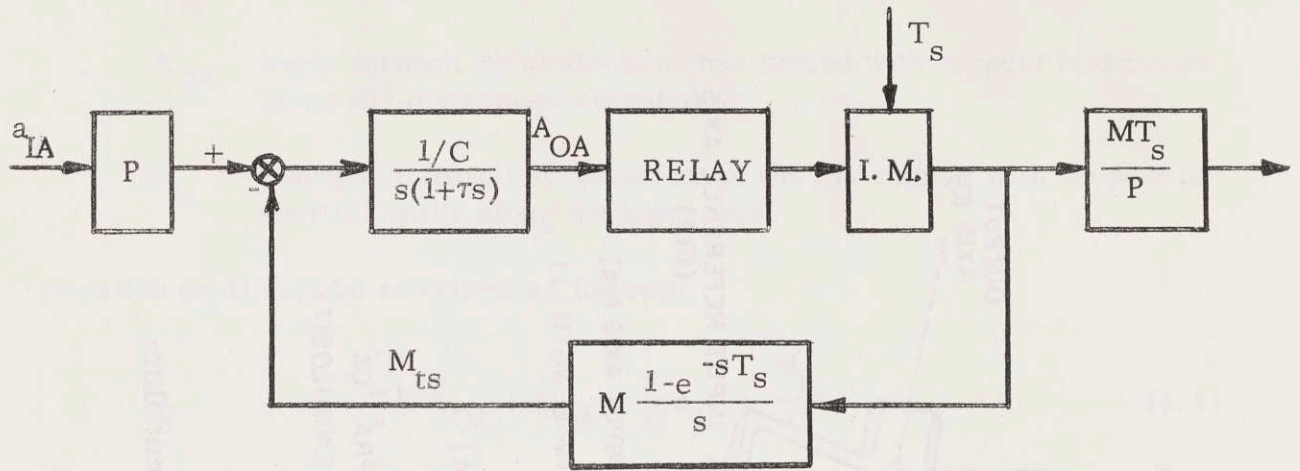


Fig. 4-7 Delta-Modulated Accelerometer.

pointed out by Wiener in Ref. (3), thus, the choice of a non limit cycling accelerometer is very attractive.

#### 4.4 Delta-Modulated Accelerometer with Three-Level Relay

A delta-modulated accelerometer with a three-level relay is shown in Fig. 4.8.

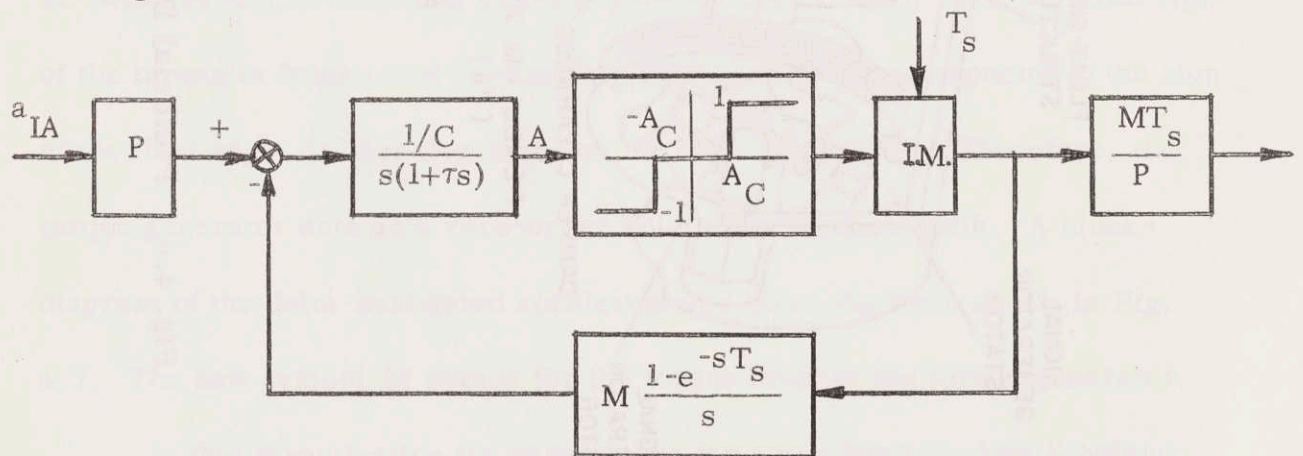


Fig. 4.8 Delta-Modulated Accelerometer with Three-Level Relay

As explained in Ref. (3) there are two energy regions to be considered when

eliminating the limit cycles for zero accelerometer inputs. The same is true for small input signals of magnitude less than about half of the design maximum. One is the low-energy region for which a transient analysis is used and the other is the high-energy region which can be handled by describing function analysis. Each analysis gives a lower limit on the zero-level and the larger is chosen as the size to be used.

The low frequency oscillations are analyzed with the low-energy method which assumes that the linear plant output is at the edge of the zero level with zero derivative and that one clock pulse occurs to drive the plant back to null. The zero level has to be chosen so wide so that in an infinite time the other edge of the zero level is not reached. As the linear plant only has an integration plus a time constant the final change of  $A$  caused by a pulse will be the integral of the pulse. The zero level should therefore be larger than half of the total change caused by one pulse

$$A_C > \frac{1}{2} \cdot \frac{MT_S}{C} \quad (4.6)$$

The delta-modulated accelerometer yields pulses which are incremental changes of the velocity. The incremental change of velocity  $\delta V$  is given by

$$\delta V = \frac{MT_S}{P} \quad (4.7)$$

Substituting equation (4.7) into (4.6) yields

$$A_C > \frac{1}{2} \cdot \frac{P}{C} \delta V \quad (4.8)$$

The high-energy analysis makes use of the describing function technique. A three-level relay has the following describing function

$$N(A) = \frac{4}{\pi A} \sqrt{1 - \left(\frac{A_C}{A}\right)^2} \quad (4.9)$$

This function has a maximum for  $A = \sqrt{2} A_C$

$$N(A)_{\max} = N(\sqrt{2} A_C) = \frac{2}{\pi A_C} \quad (4.10)$$

and  $-1/N$  will get a minimum. If the width of the zero level is chosen big enough there will be no intersection between  $-1/N$  and the extended plot of the linear plant  $G(j\omega)$ . The magnitude of the linear plant for a n-n mode, whose frequency is  $\omega_s/2n$ , is given by

$$\left|G(j \frac{\omega_s}{2n})\right| = \frac{M}{C \left|j \frac{\omega_s}{2n} (1 + j\tau \frac{\omega_s}{2n})\right|} = \frac{MT_s \cdot n}{C\pi \left[1 + \left(\frac{\pi\tau}{nT_s}\right)^2\right]^{\frac{1}{2}}} \quad (4.11)$$

To avoid modes of order n-n and lower the following must hold

$$\left|G(j \frac{\omega_s}{2n})\right| < \left|-\frac{1}{N}\right| \quad (4.12)$$

Substituting equations (4.10) and (4.11) into (4.12) yields

$$A_C > \frac{1}{2} \cdot \frac{MT_s}{C} \cdot \left\{ \frac{4n}{\pi^2} \cdot \left[1 + \left(\frac{\pi\tau}{nT_s}\right)^2\right]^{-\frac{1}{2}} \right\} \quad (4.13)$$

The factor multiplying  $\frac{1}{2} \frac{MT_s}{C}$  determines if the low or high-energy analysis gives the largest zero level width. Only the 1-1 and 2-2 modes are possible if

$$T_s > 3 \cdot \tau \quad (4.14)$$

and this is often the case as accelerometers have time constants of the order



$10^{-4}$  sec. If equation (4.14) holds and the input to the accelerometer is small, the low-energy analysis defines the smallest width of the three level relay and equation (4.6) gives the size.

#### 4.5 Increment Size and Clock Frequency

An appropriate way to determine the increment size is to analyze a "worst possible" case. If a delta-modulated accelerometer of the type described in Section 4.4 is used the maximum velocity error will be  $\frac{1}{2} \delta V$ . If the allowable error in position is  $E$  and the total flight time of the navigation  $T_n$ , then the incremental size is determined by

$$\frac{1}{2} \delta V \cdot T_n = E \quad (4.15)$$

The clock frequency  $f$  is calculated from the maximum acceleration  $a_{\max}$ ,

$$f = \frac{a_{\max}}{\delta V} \quad (4.16)$$

The sampling period is given by

$$T_s = \frac{1}{f} \quad (4.17)$$

Appropriate numbers for the reentry are

$$\begin{aligned} a_{\max} &= 10g = 322 \text{ ft/sec}^2 \\ T_n &= 36 \text{ min} \\ E &= 1 \text{ nm} \end{aligned} \quad (4.18)$$

Substitution gives

$$\delta V = 5.6 \rightarrow 5.0 \text{ ft/sec}$$

$$f = 64.4 \rightarrow 70 \text{ cps}$$

$$T_s = 1.43 \cdot 10^{-2} \text{ sec} \quad (4.19)$$

An accelerometer with that clock frequency can easily be adapted to a DDA - computer which has a bit rate of several megacycles.

#### 4.6 A Non-Linear Model for the Delta-Modulated Accelerometer

The sampling time derived in the preceding section is of such order of magnitude that equation (4.14) holds and the accelerations during the control will be less than half of the maximum acceleration for the accelerometer. It is therefore possible to use equation (4.6) when designing the three level relay for the accelerometer to be used in the range and lateral control systems. The zero level should be chosen as small as possible and  $A_C$  will therefore be kept at the edge of what equation (4.6) accepts. That means that  $2A_C$  will correspond to the final angular change caused by a pulse.

For the upcoming analysis of the range control with respect to limit cycles, it would be very handy if there was a simple model for the delta-modulated accelerometer. The model need only hold for frequencies less than 1 rad/sec. as will be shown later. In Fig. 4.9 the delta modulated accelerometer is redrawn to make it easier to explain the non-linear model of the accelerometer. The blocks inside the dotted line will be replaced by the model.

The time constant  $\tau$  is much smaller than  $T_s$

$$\frac{T_s}{\tau} \approx 143 \quad (4.20)$$

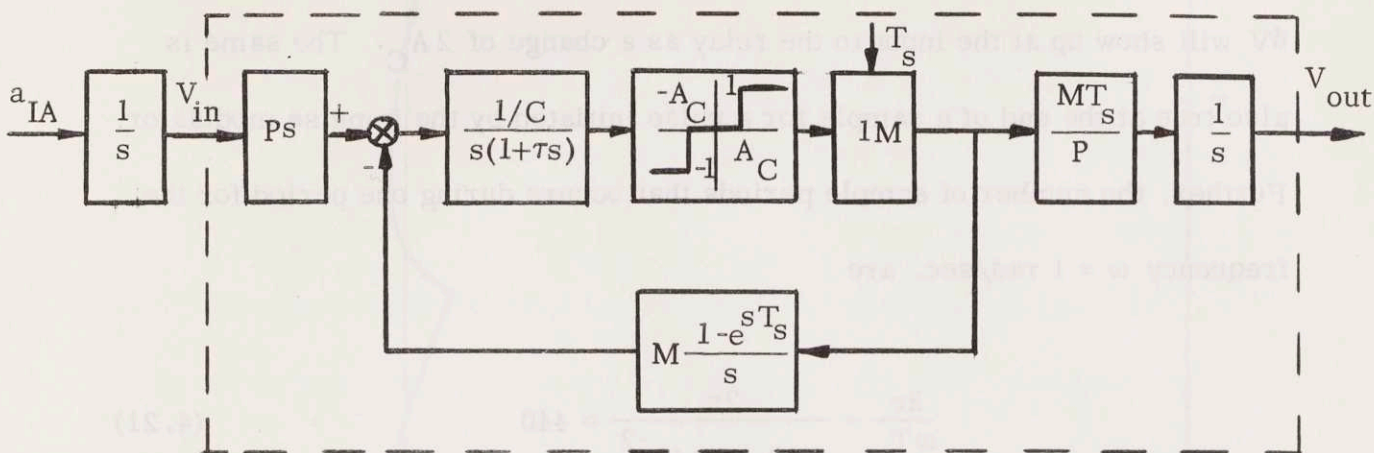


Fig. 4.9 Delta-Modulated Accelerometer Plus Integrator.

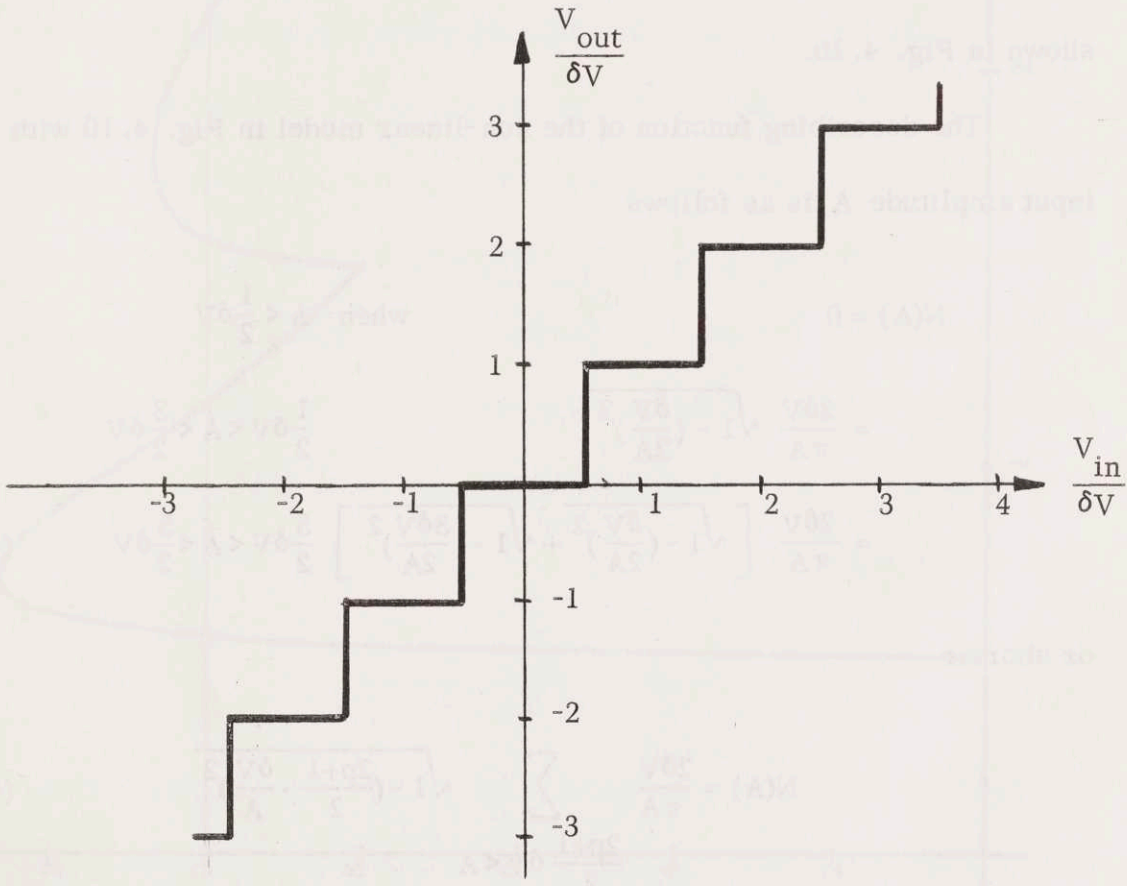


Fig. 4.10 Low Frequency Model of Delta-Modulated Accelerometer.

so  $\tau$  may be neglected in the following. Every change in  $V_{in}$  of magnitude  $\delta V$  will show up at the input to the relay as a change of  $2A_C$ . The same is also true at the end of a sample for a pulse initiated by the impulse modulator. Further, the number of sample periods that occurs during one period for the frequency  $\omega = 1$  rad/sec. are

$$\frac{2\pi}{\omega T_s} = \frac{2\pi}{1 \cdot 1.43 \cdot 10^{-2}} \approx 440 \quad (4.21)$$

The resolution due to sampling will therefore be very good for input signals with frequencies less than 1 rad/sec. and amplitudes within the limits for the accelerometer. The input to output relation of the block, indicated with the dotted lines in Fig. 4.8, may thus be represented by a quantizer of the form shown in Fig. 4.10.

The describing function of the non-linear model in Fig. 4.10 with input amplitude  $A$  is as follows

$$\begin{aligned} N(A) &= 0 && \text{when } A < \frac{1}{2}\delta V \\ &= \frac{2\delta V}{\pi A} \sqrt{1 - \left(\frac{\delta V}{2A}\right)^2} && \frac{1}{2}\delta V < A < \frac{3}{2}\delta V \\ &= \frac{2\delta V}{\pi A} \left[ \sqrt{1 - \left(\frac{\delta V}{2A}\right)^2} + \sqrt{1 - \left(\frac{3\delta V}{2A}\right)^2} \right] && \frac{3}{2}\delta V < A < \frac{5}{2}\delta V \end{aligned} \quad (4.22)$$

or shorter

$$N(A) = \frac{2\delta V}{\pi A} \sum_{\frac{2p+1}{2}\delta V < A} \sqrt{1 - \left(\frac{2p+1}{2} \cdot \frac{\delta V}{A}\right)^2} \quad (4.23)$$

where

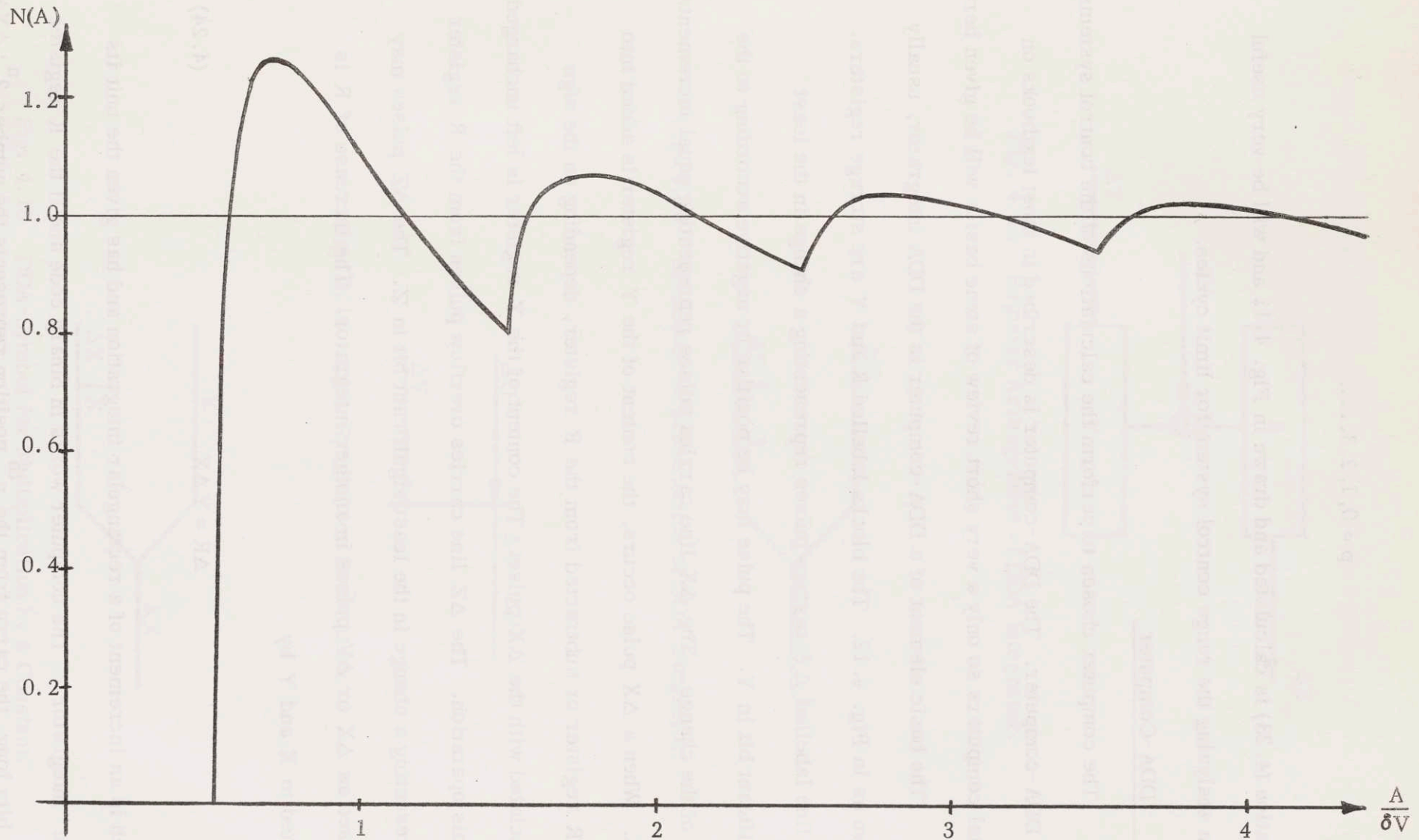


Fig. 4.11 Describing Function.

$$p = 0, 1, 2, 3, \dots$$

Equation (4.23) is calculated and drawn in Fig. 4.11 and will be very useful when analyzing the range control system for limit cycles.

#### 4.7 DDA-Computer

The computer chosen to perform the calculations of the control systems is a DDA-computer. The DDA-computer is described in most textbooks on digital computers so only a very short review of some basics will be given here.

The basic element of a DDA-computer is the DDA integrator, usually shown as in Fig. 4.12. The blocks labelled R and Y are storage registers. The line labelled  $\Delta Y$  carries pulses representing a change in the least significant bit in Y. The pulse may be positive or negative according to the sign of the change. The  $\Delta X$  line carries pulses representing equal increments in X. When a  $\Delta X$  pulse occurs, the content of the Y register is added into the R register or subtracted from the R register, depending on the sign associated with the  $\Delta X$  pulse. The content of the Y register is left unchanged by this operation. The  $\Delta Z$  line carries overflow pulses from the R register representing a change in the least significant bit in Z. The  $\Delta Z$  pulses may be used as  $\Delta X$  or  $\Delta Y$  pulses in another integrator. The increase of R is related to X and Y by

$$\Delta R = Y \Delta X \quad (4.24)$$

which is an increment of a rectangular integration and has given the unit its name "integrator." The computer works in binary code and if the R register is n bits long, the carry from the  $n^{\text{th}}$  position represents the number  $2^n \cdot \Delta X \Delta Y$ .

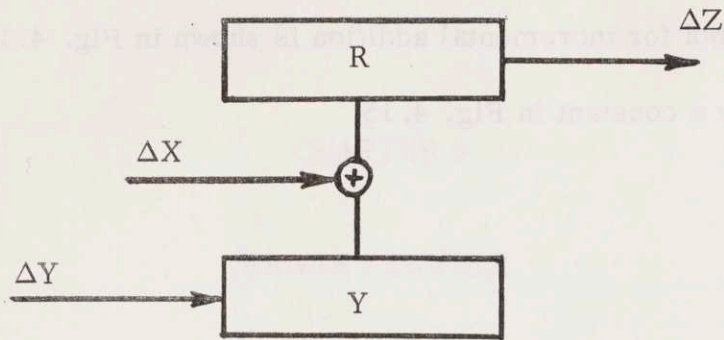


Fig. 4.12 Register Arrangement of DDA Integrator.

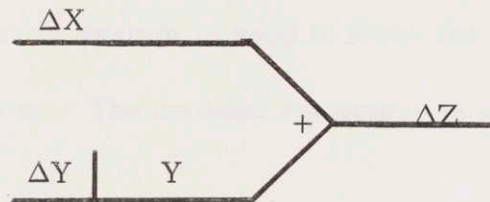


Fig. 4.13 Schematic Representation of DDA Integrator.

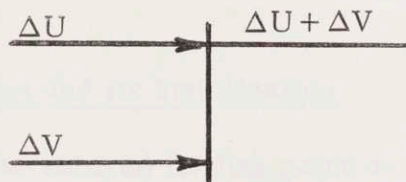


Fig. 4.14 DDA-Symbol for Summation.

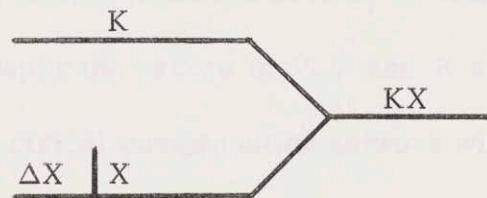
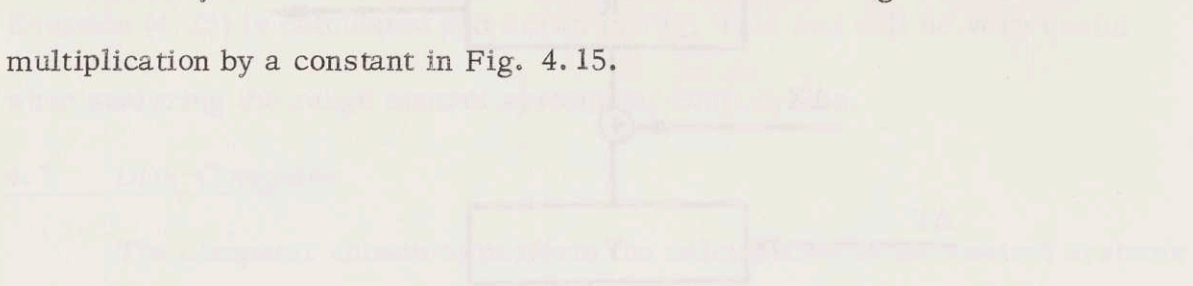


Fig. 4.15 DDA-Symbol for Multiplication by a Constant.

The usual schematic representation for a DDA integrator is shown in Fig. 4.13.

The symbol for incremental addition is shown in Fig. 4.14 and multiplication by a constant in Fig. 4.15.



The basic element of a DDA computer is the DDA integrator, usually shown as in Fig. 4.13. The input to the DDA integrator is the derivative of the function to be integrated. The DDA integrator is designed to approximate the integral of the input signal by using a digital computer. The DDA integrator is usually shown as in Fig. 4.13. The input to the DDA integrator is the derivative of the function to be integrated. The DDA integrator is designed to approximate the integral of the input signal by using a digital computer.



Fig. 4.13. DDA symbol for differentiation by a constant.



## CHAPTER 5

### RANGE CONTROL

#### 5.1 Introduction

To guide the vehicle during the Landing Phase so that it will reach the destination area, a range control system is used to force the vehicle to follow a reference or nominal trajectory. The nominal trajectory is generated with time as the independent variable.

The range control is first stabilized for continuous signals. Then, a delta modulated accelerometer and a DDA is introduced in the control system and analysis is carried out to find if the delta modulated accelerometer gives rise to any limit cycles.

#### 5.2 The Range Control System and Its Stabilization

To guide the vehicle to the desired landing point on the earth the difference between actual distance to go and nominal flight distance can be used as an error signal in a control system operating on the ratio  $(L/D)_v$ . To stabilize the range control system it is also necessary to include other correction signals. In this paper the errors in  $\dot{V}$ ,  $V$  and  $R$  away from the nominal trajectory and an electrical compensation network will be used to govern the lift as shown in Fig. 5.1. The block called Nominal trajectory generates the equations derived in Chapter 2 using  $t$  as independent variable.

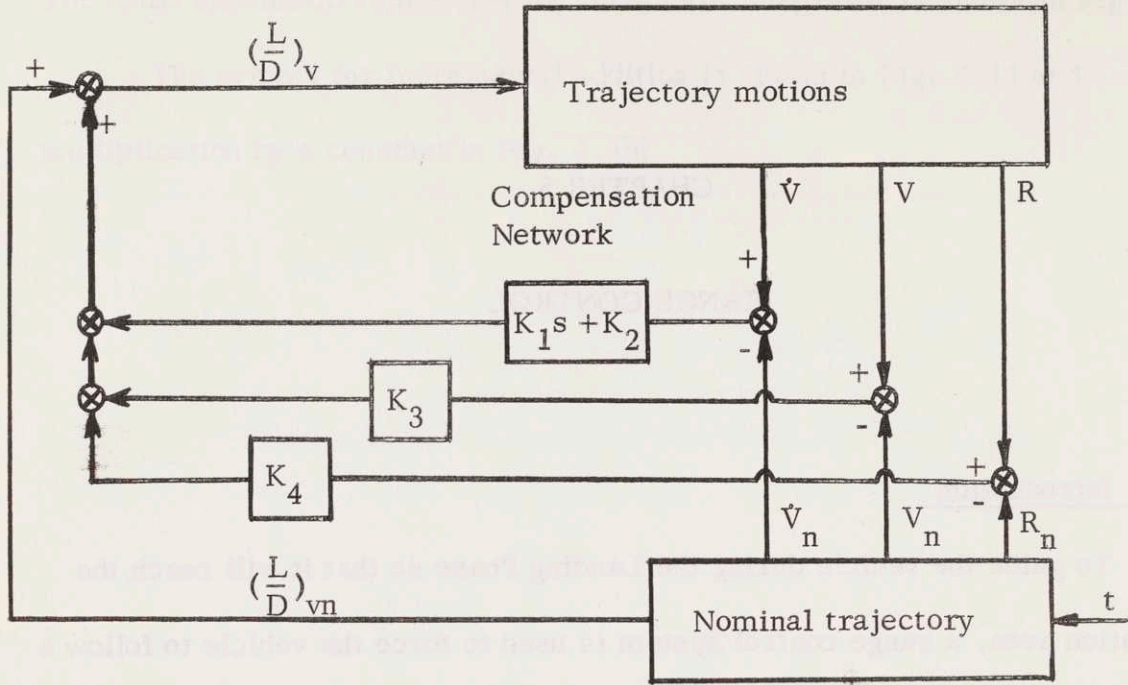


Fig. 5.1 Range Control System.

The nominal value of  $(L/D)_v$  is a constant and so are the feedback gains  $K_1, K_2, K_3$  and  $K_4$ .

The guidance law for the system is

$$\left(\frac{L}{D}\right)_v = \left(\frac{L}{D}\right)_{vn} + (K_1s + K_2)\Delta\dot{V} + K_3\Delta V + K_4\Delta R \dots \quad (5.1)$$

where the  $\Delta$ -quantities represent the variations of the measured variables from the nominal values along the trajectory.

The transfer functions for the trajectory dynamics are derived in Chapter 3 giving equation (3.52). For convenience introduce the following notations.

$$\frac{\Delta\dot{V}}{\Delta\left(\frac{L}{D}\right)_v} = \frac{K_0}{s^2 + \omega_0^2} \quad (5.2)$$

where

$$K_0 = \frac{\beta g^2 (1 - \bar{V}^2)^2}{\left(\frac{L}{D}\right)_{vn}^2} \quad (5.3)$$

$$\omega_0^2 = \beta g (1 - \bar{V}^2) \quad (5.4)$$

Using the notations of equation (5.2)-(5.4) a block diagram of the range control system is drawn in Fig. 5.2.

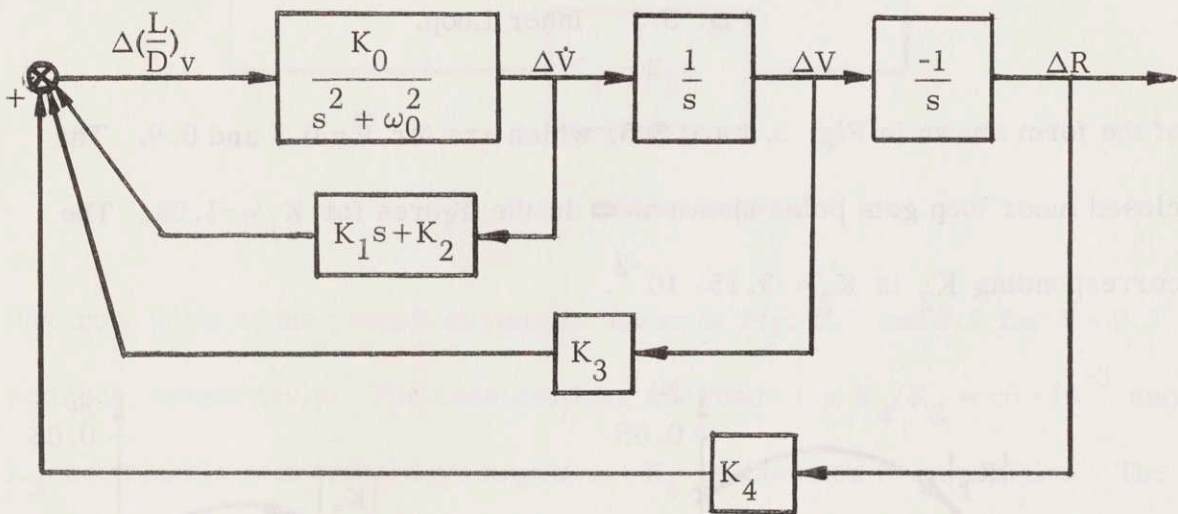


Fig. 5.2 Block Diagram of Range Control System.

To stabilize the range control system Root-locus technique is applied. First the inner loop of Fig. 5.2 containing the compensation network is stabilized.

Fig. 5.3 shows the inner loop itself. The characteristic function of the inner loop is

$$1 - \frac{K_0(K_1s + K_2)}{s^2 + \omega_0^2} = 1 - \frac{K_0K_1\left(s + \frac{K_2}{K_1}\right)}{s^2 + \omega_0^2} \quad (5.5)$$

Choosing  $K_1$  and  $K_2$  negative and the ratio  $K_2/K_1 = 3 \cdot 10^{-2}$  gives root-loci

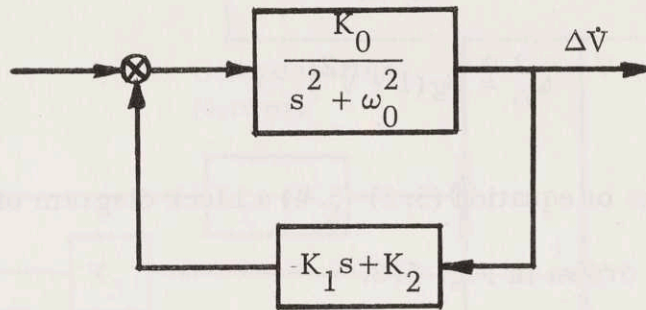


Fig. 5.3 Inner Loop.

of the form shown in Fig. 5.4 and 5.5, which are for  $\bar{V} = 0.3$  and  $0.9$ . The closed inner loop gets poles shown as  $\square$  in the figures for  $K_1 = -1.05$ . The corresponding  $K_2$  is  $K_2 = -3.15 \cdot 10^{-2}$ .

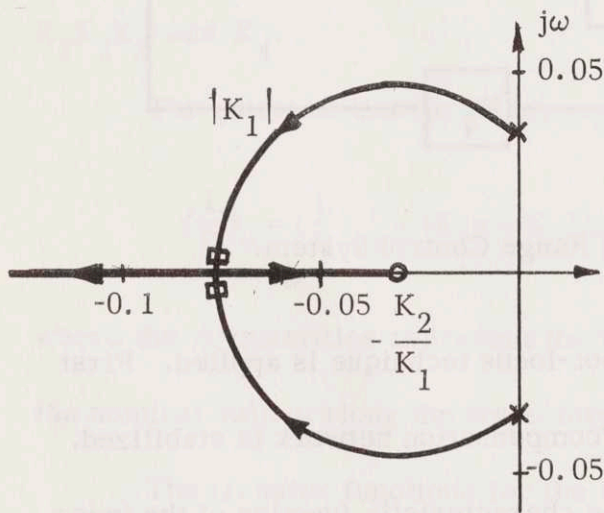


Fig. 5.4 Root-Locus for Inner Loop,  $\bar{V} = 0.30$ .

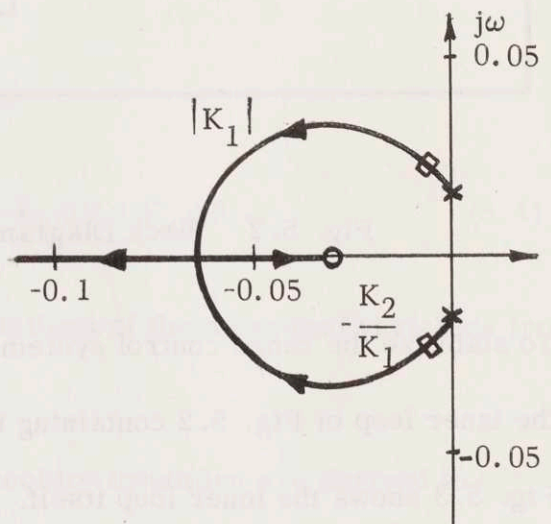


Fig. 5.5 Root-Locus for Inner Loop,  $\bar{V} = 0.90$ .

The inner loop is thus stable. The overall range control system of Fig. 5.2 can now be treated as a system containing the inner loop as a single block.

Further, the two feedback loops with the constants  $K_3$  and  $K_4$  may be lumped together into one single feedback loop. Redrawing the control system of Fig. 5.2 in that way transforms it into Fig. 5.6.

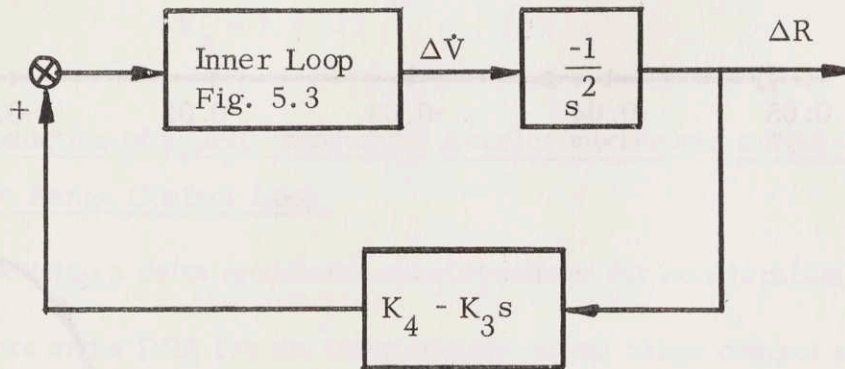


Fig. 5.6 Outer Loop.

The root locus of the overall system is shown in Fig. 5.7 and 5.8 for  $\bar{V} = 0.3$  and 0.9, respectively. The constructions are made for  $K_4/K_3 = -6 \cdot 10^{-3}$  and  $K_3$  as variable gain and always negative.  $K_4$  is assumed to be positive. The final choice of  $K_3$  is  $K_3 = -3 \cdot 10^{-4}$  which determines that  $K_4 = 1.8 \cdot 10^{-6}$ .

The poles of the overall range control system with these values of the constants are shown as  $\blacksquare$  in Fig. 5.7 and 5.8.

The figures show that the range control system is stable with the values that have been chosen for  $K_1 K_2 K_3$  and  $K_4$ . At the beginning of the landing maneuver the damping is not very good but gets better during the approach to the landing point. No analysis of the signal amplitudes due to initial errors will be carried out in this report.

The range control system designed in this section is of the form shown in Fig. 5.1 and 5.2. The values of the feedback constants that have been

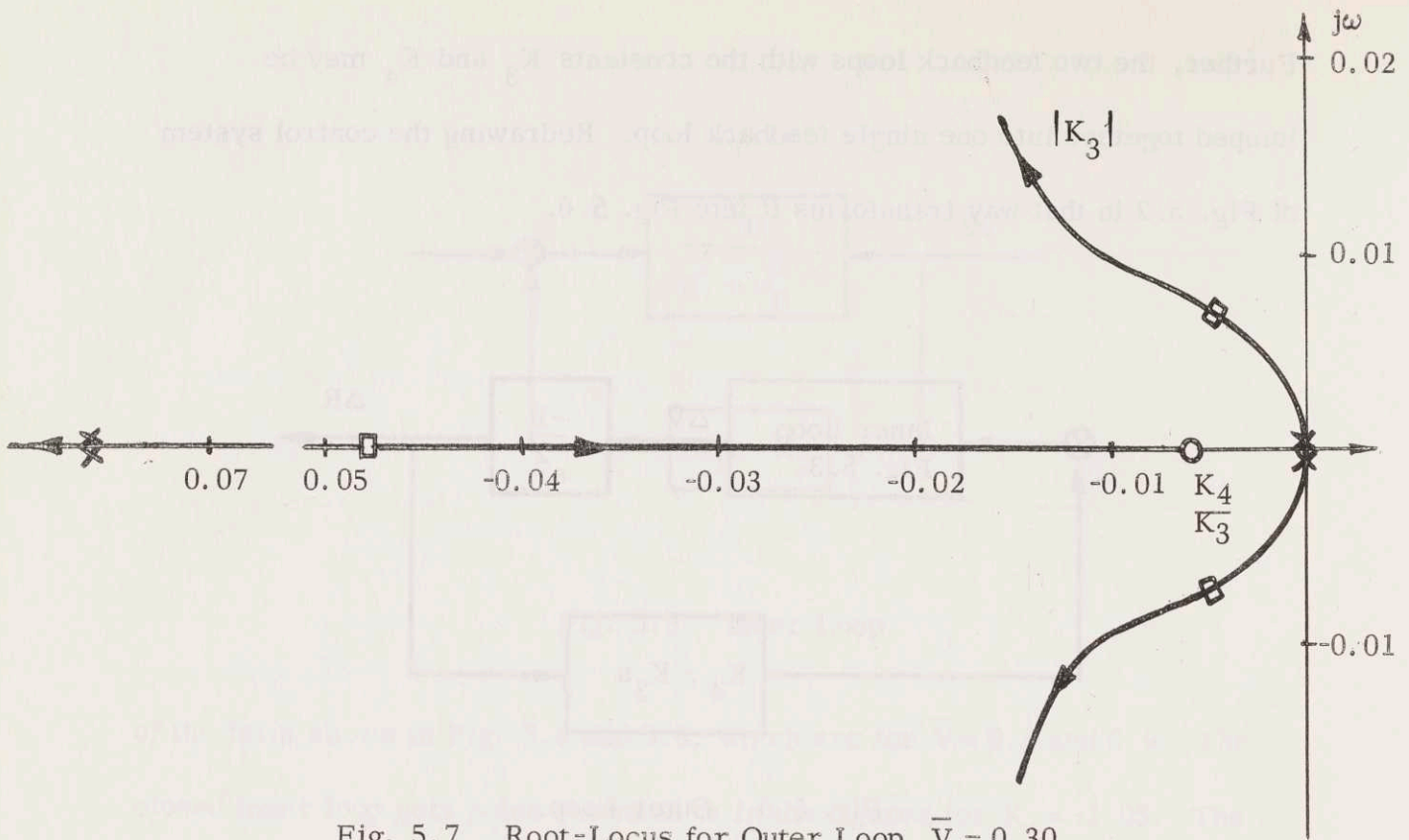


Fig. 5.7 Root-Locus for Outer Loop,  $\bar{V} = 0.30$ .

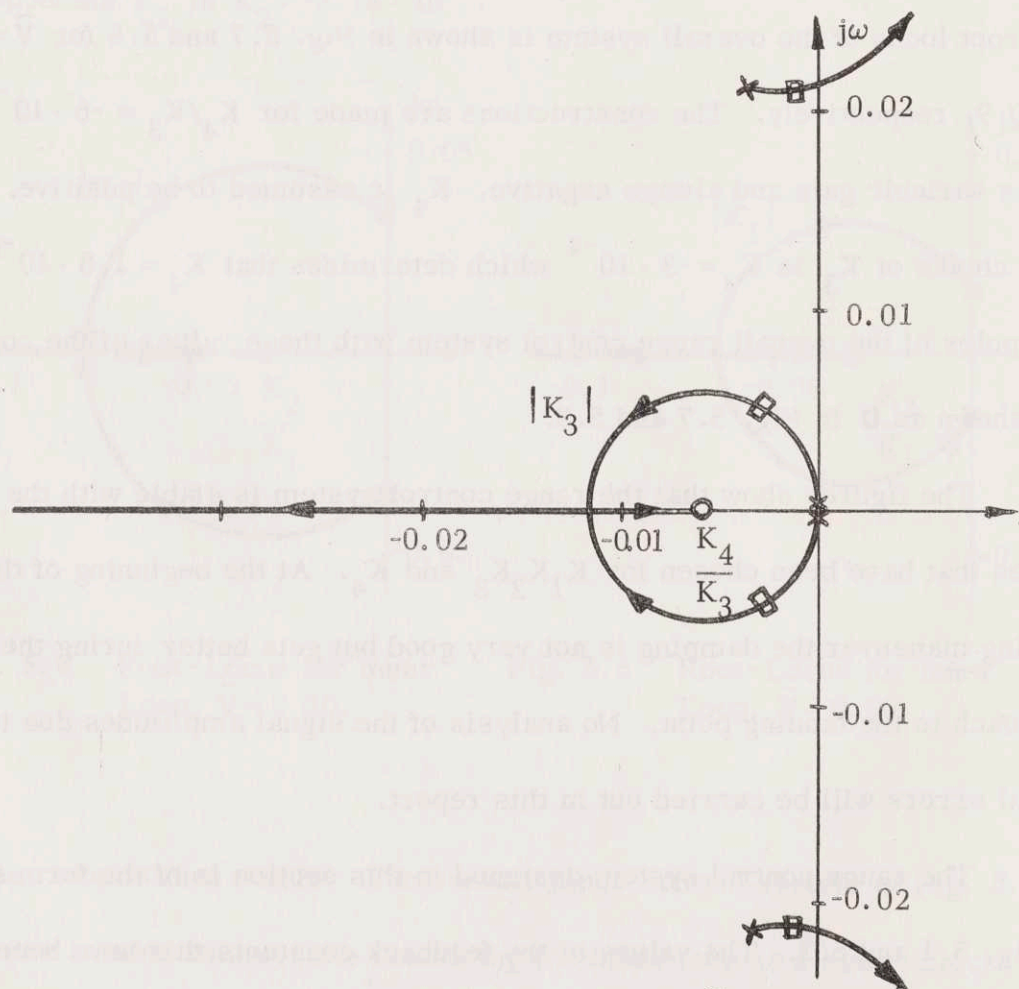


Fig. 5.8 Root-Locus for Outer Loop,  $\bar{V} = 0.90$ .

chosen are as follows

$$\begin{aligned}
 K_1 &= -1.05 && 1/\text{fps}^3 \\
 K_2 &= -3.15 \cdot 10^{-2} && 1/\text{fps}^2 \\
 K_3 &= -3 \cdot 10^{-4} && 1/\text{fps} \\
 K_4 &= 1.8 \cdot 10^{-6} && 1/\text{ft}
 \end{aligned} \tag{5.6}$$

### 5.3 Introduction of a Delta-Modulated Accelerometer and a DDA-Computer in the Range Control Loop

Introducing a delta modulated accelerometer for acceleration measurements and a DDA for the computations in the range control system of Fig. 5.2 changes the picture of the loop. Figure 5.9 shows the new setup with a zero order hold following the DDA. The delta modulated accelerometer is abbreviated DMA and the  $\Delta$ 's have been dropped. The Laplace transforms that the DDA should give is defined by Fig. 5.2 and are as follows

$$C(s) = \left( \frac{K_4}{s} - K_3 - K_2 s - K_1 s^2 \right) V(s) \tag{5.7}$$

$$V(s) = \frac{1}{s} \delta V(s) \tag{5.8}$$

There is no reason to design the DDA from any other transforms to compensate for the stepping as the sampling period is very short compared to the bandwidth of the range control system. A DDA that will approximate equations (5.7) and (5.8) very well is shown in Fig. 5.10. A z-transform will describe the behaviour of the computer if the quantization in the computer is neglected, which is possible as the steps may be done very small. The z-transform can be derived from the difference equations that the computer solves. The clock frequency of the computer is several megacycles and the sampling time

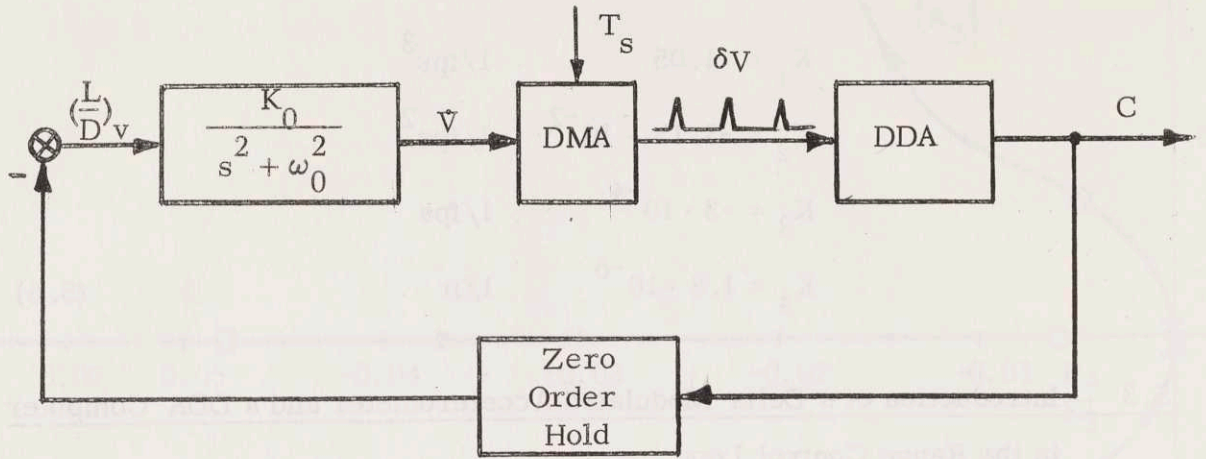


Fig. 5.9 Range Control Loop with DMA and DDA.

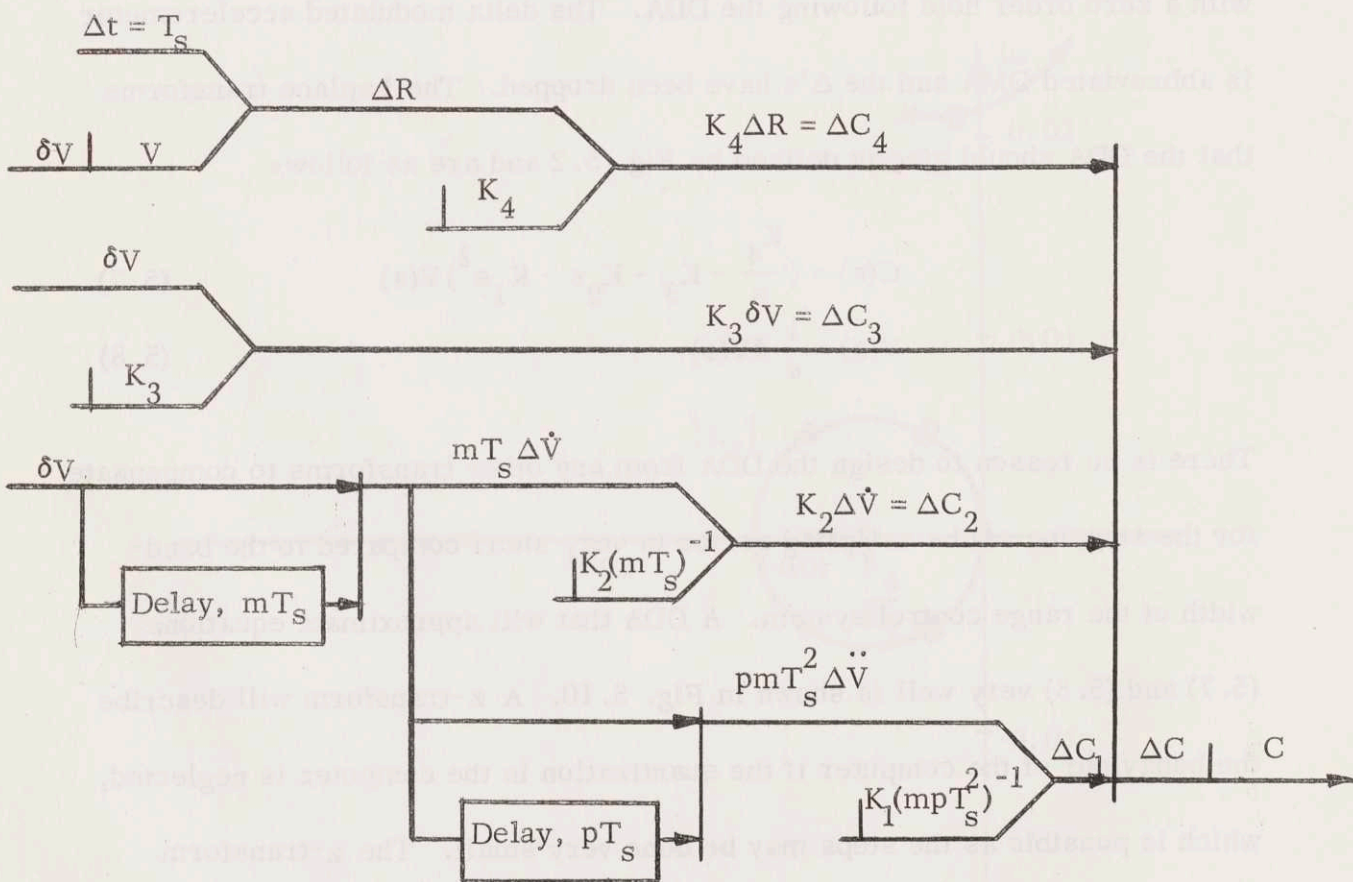


Fig. 5.10 Illustration of DDA-Program.



is  $T_s = 1.43 \cdot 10^{-2}$  sec., thus there is no need for delays between the operations of the computer. The derivatives are calculated by taking the difference between a variable of present time and a delayed value of the same variable and divide by the time difference between the samples. The difference equations are as follows if the notations of Fig. 5.10 are used.

$$\begin{aligned}
 V(n) &= V(n-1) + \delta V(n) \\
 \Delta R(n) &= T_s V(n-1) \\
 R(n) &= R(n-1) + \Delta R(n) \\
 C_4(n) &= K_4 R(n) \\
 C_3(n) &= -K_3 V(n) \\
 \dot{V}(n) &= 1/mT_s [V(n) - V(n-m)] \\
 C_2(n) &= -K_2 \dot{V}(n) \\
 \ddot{V}(n) &= 1/pT_s [\dot{V}(n) - \dot{V}(n-p)] \\
 C_1(n) &= -K_1 \ddot{V}(n) \\
 C(n) &= C_1(n) + C_2(n) + C_3(n) + C_4(n)
 \end{aligned}$$

Introducing the  $z$ -variable as

$$z = e^{sT_s} \quad (5.10)$$

and solving equation (5.9) for  $C(z)$  gives

$$\begin{aligned}
 C(z) = & \left[ K_4 \frac{T_s}{z-1} - K_3 - K_2 \frac{1}{mT_s} (1-z^{-m}) + \right. \\
 & \left. -K_1 \frac{1}{pmT_s^2} (1-z^{-p})(1-z^{-m}) \right] \frac{z}{z-1} \delta V(z) \quad (5.11)
 \end{aligned}$$

The  $z$ -transform of the computer  $D(z)$  is thus

$$D(z) = \left[ K_4 \frac{T_s}{z-1} - K_3 - K_2 \frac{1}{mT_s} (1-z^{-m}) - K_1 \frac{1}{pmT_s^2} (1-z^{-p})(1-z^{-m}) \right] \frac{z}{z-1} \quad (5.12)$$

To eliminate noise from the quantizing of the accelerometer a filter should be included in the computer to attenuate high frequencies. A sharp filter with a bandwidth of about 1 rad/sec. should probably work well, but will not be designed here.

The Laplace-transform for the zero order hold is of the form

$$G_{oh} = \frac{1 - e^{-sT_s}}{s} \quad (5.13)$$

The delta modulated accelerometer has already been discussed in the preceding chapter and the range system can now be analyzed for limit cycles.

#### 5.4 Limit Cycles

When analyzing the range control system with respect to limit cycles, Fig. 5.11 will be used. The inner loop is the accelerometer loop and the outer loop is the range control loop. The analysis will be performed in two steps. In the first step high frequencies will be discussed and in the second step low frequencies.

When analyzing the system for high frequency limit cycles the gain of the two loops will first be compared between point 1 and 2 in Fig. 5.11. If leaving out the zero order holds which appear in both loops the following inequality is true for high frequencies.

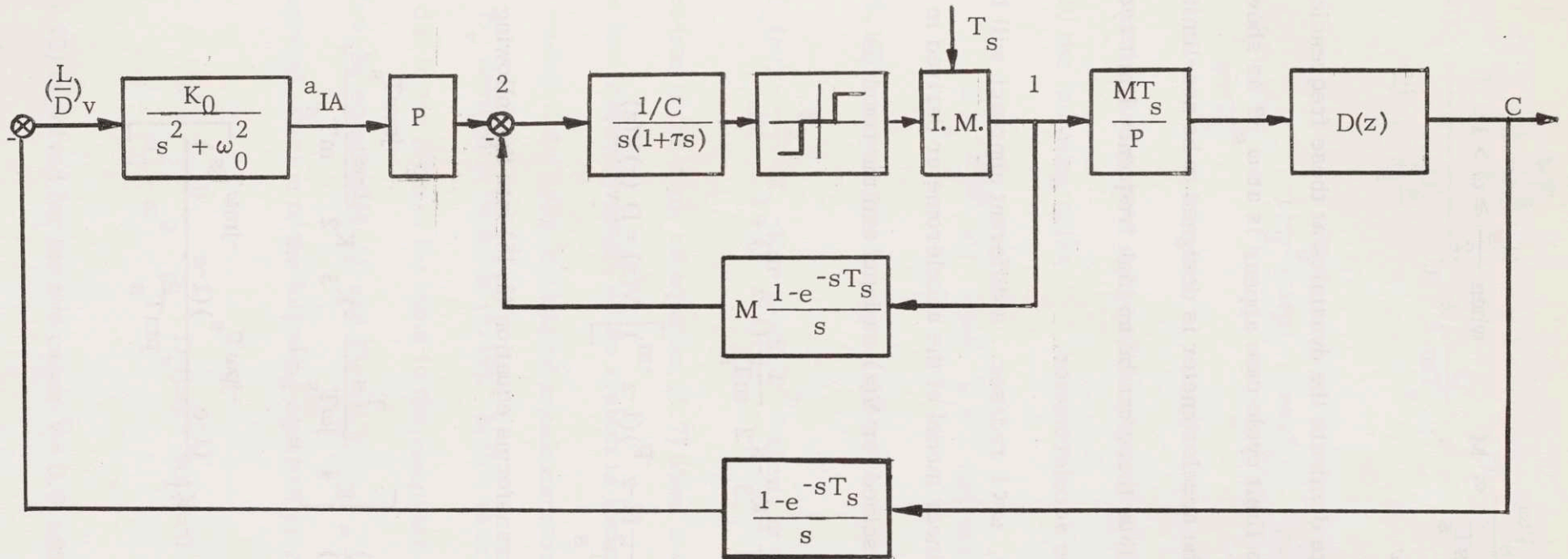


Fig. 5.11 Range Control Loop with Delta-Modulated Accelerometers.

$$\left| MT_s D(z) \frac{K_0}{s^2 + \omega_0^2} \right|_{\substack{z=e^{sT_s} \\ s=j\omega}} \ll M \quad \text{when } \frac{\omega_s}{2} \geq \omega > 1 \quad (5.14)$$

The inner loop will therefore dominate the dynamics at these frequencies. The highest frequency at which a limit cycle can appear is at  $\omega_s/2$  as shown in Section 4.2.2. However, the accelerometer is designed to be non-limit cycling for small input signals and thus there can be no high frequency limit cycle in the range control loop due to the accelerometer.

For low frequencies,  $\omega < 1$  rad/sec., a different approach will be carried out making use of the non-linear model of the accelerometer derived in Section 4.6. Equation (5.9) can be solved for  $V(z)$  as input and the result is

$$C(z) = \left[ K_4 \frac{T_s}{z-1} - K_3 - K_2 \frac{1}{mT_s} (1-z^{-m}) + \right. \\ \left. - K_1 \frac{1}{pmT_s^2} (1-z^{-p})(1-z^{-m}) \right] V(z) = D_v(z)V(z) \quad (5.15)$$

Substituting  $z$  with  $e^{j\omega T_s}$  transforms equation (5.15) into the following transfer function

$$D_v(j\omega) = \frac{C(j\omega)}{V(j\omega)} = \left[ K_4 \frac{T_s}{e^{j\omega T_s} - 1} - K_3 - K_2 \frac{1 - e^{-jm\omega T_s}}{mT_s} + \right. \\ \left. - K_1 \frac{(1 - e^{-jp\omega T_s})(1 - e^{-jm\omega T_s})}{pmT_s^2} \right] \quad (5.16)$$

Trigonometric relations give

$$\begin{aligned}
D_v(j\omega) = & K_4 \frac{T_s e^{-j \frac{\omega T_s}{2}}}{2j \sin \frac{\omega T_s}{2}} - K_3 - K_2 \frac{2j}{m T_s} \cdot e^{-j \frac{m \omega T_s}{2}} \sin \frac{m \omega T_s}{2} + \\
& + K_1 \frac{4}{pm T_s^2} \cdot e^{-j \frac{\omega T_s}{2} (m+p)} \sin \frac{m \omega T_s}{2} \sin \frac{p \omega T_s}{2} \quad (5.17)
\end{aligned}$$

The constants  $m$  and  $p$  have not yet been chosen. If they are given integers less than 10 the following holds

$$\omega T_s \frac{m+p}{2} \ll 1 \quad \text{when } \omega < 1 \text{ rad/sec} \quad (5.18)$$

Equation (5.17) can therefore be approximated as follows

$$D_v(j\omega) = \frac{K_4}{j\omega} - K_3 - K_2 \cdot j\omega + K_1 \omega^2 \quad \text{when } \omega < 1 \text{ rad/sec} \quad (5.19)$$

This expression is the same as equation (5.7) when  $s = j\omega$ .

The low frequency model of the system is shown in Fig. 5.12 using the non-linear model of the delta-modulated accelerometer from Section 4.6 and the transform  $D_v$  derived in equation (5.19). In this case the zero order hold can be left out due to the form of the input to the computer. The describing function is determined by equation (4.23) and Fig. 4.10.

Graphical solution of the following equation gives the limit cycles.

$$1 + \frac{K_0}{\omega_0^2 - \omega^2} \cdot \frac{1}{j\omega} \cdot D_v(j\omega) \cdot N(A) = 0 \quad (5.20)$$

Equation (5.20) is solved for the two cases  $\bar{V} = 0.9$  and  $\bar{V} = 0.3$  in Fig. 5.13 and 5.14, respectively.

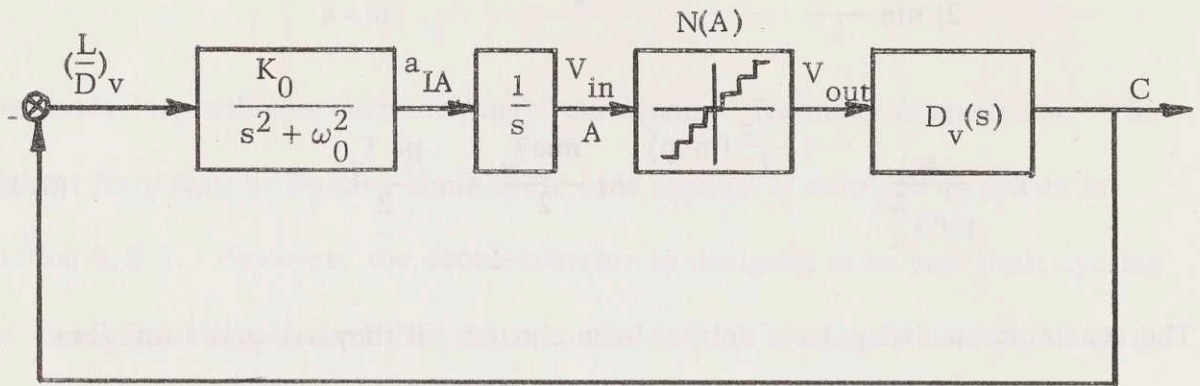


Fig. 5.12 Low Frequency Model of Range Control Loop.

Figure 5.13,  $\bar{V} = 0.9$ , has one stable limit cycle at  $\omega = 1.75 \cdot 10^{-2}$  rad/sec and  $A \approx 0.51\delta V = 2.55$  ft/sec. Figure 5.14,  $\bar{V} = 0.3$ , has no limit cycles at all and is stable.

The amplitude of  $(L/D)_v$  at the limit cycle is calculated from

$$\left(\frac{L}{D}\right)_v \cdot \left| \frac{K_0}{\omega_0^2 - \omega^2} \right| \cdot \frac{1}{\omega} = A \quad (5.21)$$

and gives the answer

$$\left(\frac{L}{D}\right)_v = 3.3 \cdot 10^{-4} \quad (5.22)$$

The relative amplitude for  $(L/D)_{vn} = 1/2$  is thus

$$\frac{\left(\frac{L}{D}\right)_v}{\left(\frac{L}{D}\right)_{vn}} = 7 \cdot 10^{-4} \quad (5.23)$$

This amplitude is acceptable and will cause no harm to the system. The

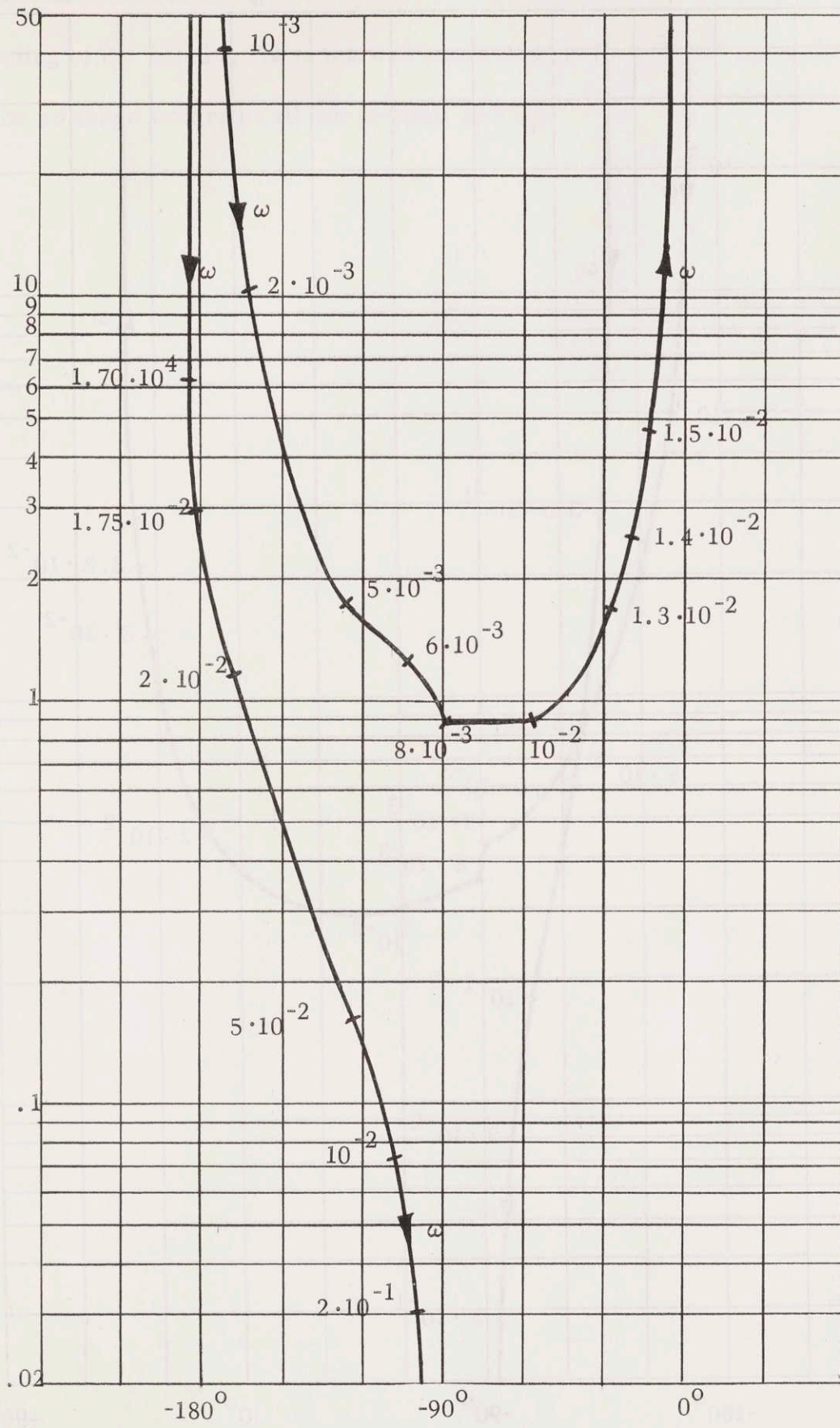


Fig. 5.13 Range Control for  $\bar{V} = 0.90$ .

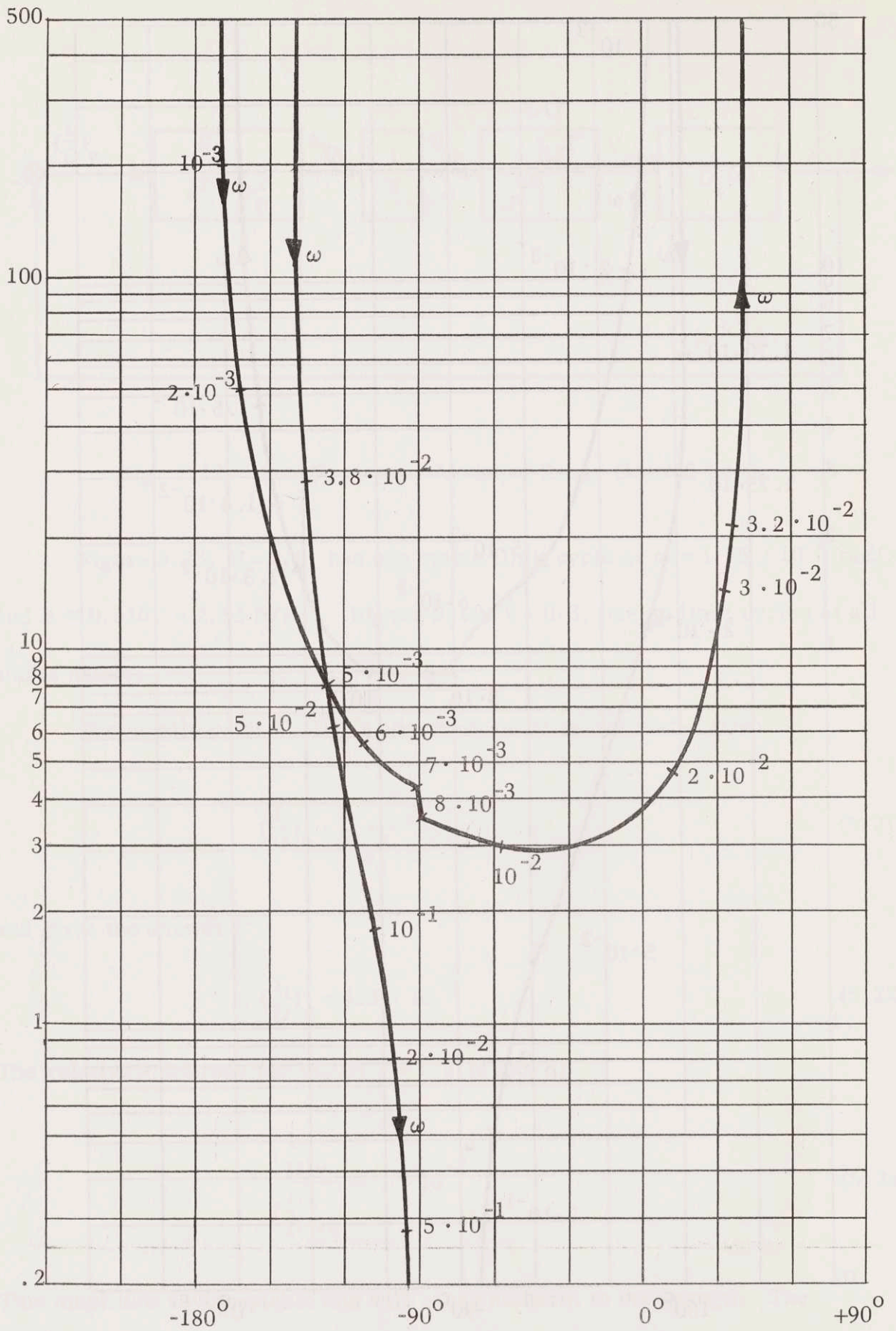


Fig. 5.14 Range Control for  $\bar{V} = 0.30$ .



conclusion is that the range control system will experience a limit cycle in the beginning of the Landing Phase but will settle down before  $\bar{V} = 0.3$ , so there will be no range errors at all due to limit cycling.

### 3.1.3 Integration

When a landing approach is initiated, the range control system will be in the cruise phase by riding the lift vector. The lift is generated by rolling the vehicle to a bank angle of  $\theta$  degrees. The lift vector is then controlled by rolling the lift vector to the right (L/R) for the range. As soon as the lift vector is rolled to the right, the lift vector will be rolled back to the left vector. The lift vector will be rolled to an angle of  $\theta$  degrees (L/R) for the range. The lateral control system will then automatically provide the speed vector error as the lift vector will be rolled back to the original cruise angle error is reached. The lift vector will automatically be rolled back to the original lift and the bank angle  $\theta$  degrees for the range. The control system will compare the range error with the range error and when the range error is zero, the lift vector will be rolled back to its original position. The procedure is then repeated until landing and landing point height is zero in the cruise range of the.

### 3.1.4 The Integral Control System

When calculating the lateral motion of the vehicle, usually with the lift vector, the lift vector can be determined by the lift vector. Figure 3.1.4

## CHAPTER 6

### LATERAL CONTROL

#### 6.1 Introduction

With a lifting vehicle it is possible to move laterally out of the vertical trajectory plane by tilting the lift vector. The tilt is obtained by rolling the vehicle by means of small control jets. As the range is also controlled by tilting the lift vector to get the right  $(L/D)_v$  for the range, lateral control has to be done by two-position control of the lift vector. The lift vector is first banked at an angle  $B$  to give a correct  $(L/D)_v$  for the range. The lateral control system will then continuously predict the cross range error at the landing point and when the maximum tolerable cross range error is reached the lift vector will immediately be rolled over to the opposite side and the bank angle  $-B$ , giving the same  $(L/D)_v$  as before. The control system will continue to predict cross range error and when the other limit of tolerable cross range error is reached the lift vector will be rolled back to its first position. The procedure is then repeated thus keeping the landing point inside the limits of the cross range error.

#### 6.2 The Lateral Control System

When calculating the lateral motion of the vehicle, usually some type of approximation has to be introduced to get useful expressions. Eggers and

Slye, Ref. (16) and (2), respectively, make use of a "cylindrical" earth. The plane which contains the nominal flight trajectory is perpendicular to the cylinder, which has the same diameter as the earth. The approximation does not give extreme accuracy if the flight path deviates widely from the nominal trajectory. The accuracy of the approximation has been discussed by Rosenbaum, Ref. (1). When the lateral motion of the vehicle is controlled, the actual flight path will be close to the nominal path and thus, the approximation will be very good. In Fig. 6.1 the flight path is depicted as seen from above looking down towards the center of the earth.

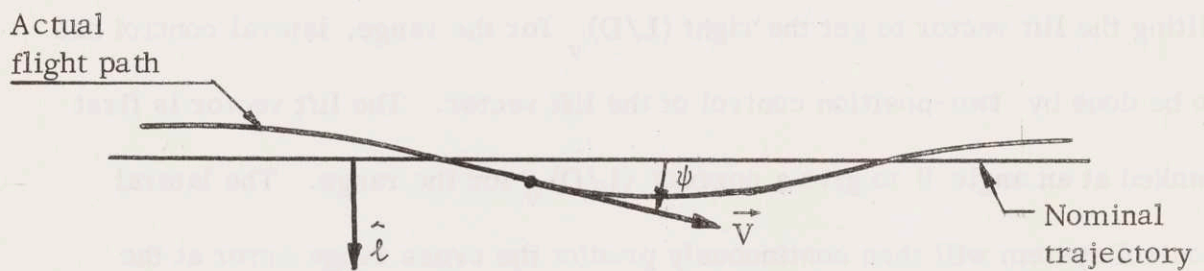


Fig. 6.1 Lateral Flight Path

The angle  $\psi$  is the bearing angle of the velocity vector with respect to the nominal trajectory. The vector  $\hat{l}$  is a unit vector of  $l$  perpendicular to the nominal flight path. The acceleration in  $l$ -direction is

$$\ddot{l} = \dot{\psi}V \cos \gamma \cos \psi \quad (6.1)$$

Making the small angle approximation gives

$$\ddot{l} = \dot{\psi}V \quad (6.2)$$

In the same way the horizontal component of lift  $L_h$  is given by the bank angle

B

$$L_h = L_v \tan B \quad (6.3)$$

The equations of motion perpendicular to the nominal trajectory are

$$m\dot{\psi}V = L_v \tan B \quad (6.4)$$

and

$$m\ddot{\ell} = L_v \tan B \quad (6.5)$$

The rate of change of the bearing angle is found from equation (6.4)

$$\dot{\psi} = \frac{L_v \tan B}{mV} \quad (6.6)$$

and the lateral position from equation (6.5)

$$\ell = \iint \frac{L_v \tan B}{m} dt^2 \quad (6.7)$$

The cross range error at the landing point for a vehicle which is not banked is shown in Fig. 6.2 as  $\ell_f$ . The distance from the vehicle to nominal trajectory at the initial point is called  $\ell$  and the range to go is S, equation (2.16).

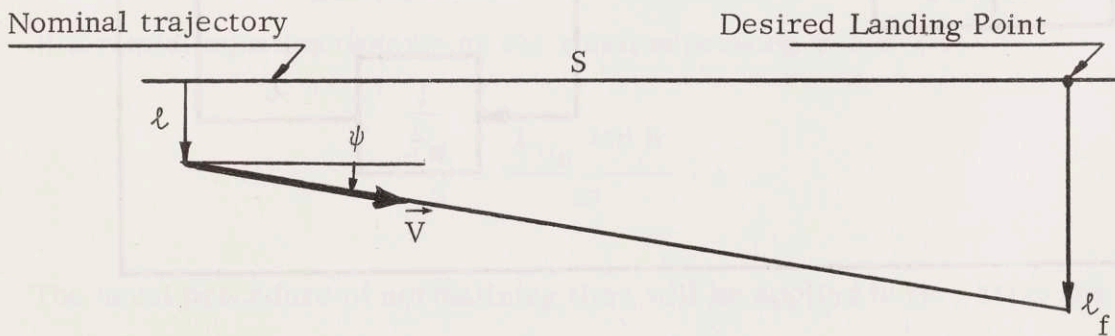


Fig. 6.2 Prediction of Cross Range Error

Figure 6.2 gives the following equation for the cross range error at the landing point

$$l_f = l + \psi \cdot S \quad (6.8)$$

if, again, the small angle approximation is used.

The cross range error  $l_f$  of equation (6.8) can be used to control the bank angle of the vehicle. When  $l_f$  has increased to the maximum tolerable cross range error  $l_m$  the lift vector is rolled over to the other side where it stays until the other limit is reached. The rolling of the vehicle is obtained by control jets which can roll the vehicle from  $-90^\circ$  to  $90^\circ$  in 10 seconds. The time between two successive changes of the bank angle will be about 1 minute or more and the bank angle used will be about  $30^\circ$ . The switching of the bank angle from one side to the other will therefore be very fast compared to the time between two switches of the bank angle and can be approximated to be instantaneous. If that approximation is used, the analytic model of the lateral control system for different points along the flight path is of the form shown in Fig.

6.3.

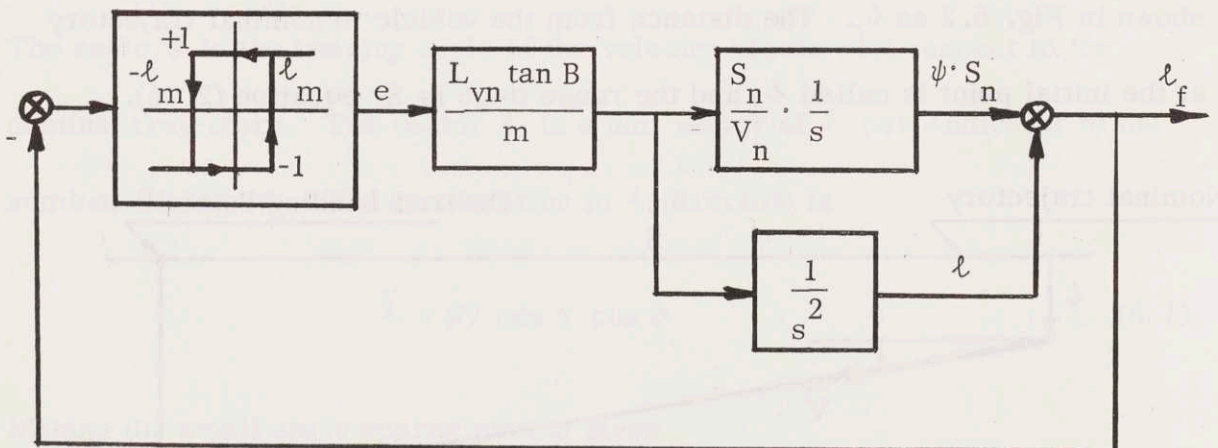


Fig. 6.3 Lateral Control System

In Fig. 6.3 the subscript n denotes values along the nominal trajectory and the point where the lateral control system is being analyzed. The notation e has the value +1 or -1 and s is the Laplace operator.

It is of interest to know if the lateral control system has a limit cycle or not and if all initial conditions will give the limit cycle if the system has one. The usual way of analyzing the system is to use describing function technique. However, that cannot be used for this control system as the filtering of the linear part of the system is not enough. The phase-plane method will, instead, give information about transients and limit cycles. To get the control system in a form suitable for phase-plane analysis, Fig. 6.3 has been redrawn in Fig. 6.4.

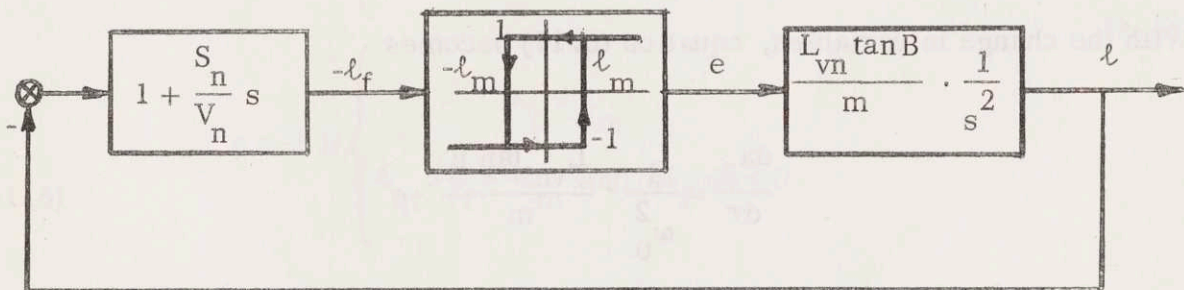


Fig. 6.4 Block Diagram For Phase Plane Analysis

The first step in constructing the phase-plane is to write the differential equation describing the relation between e and l.

$$\frac{d^2 l}{dt^2} = \frac{L_{Vn} \tan B}{m} \cdot e \quad (6.9)$$

The usual procedure of normalizing time will be applied here. Make the following change in the time scale

$$\tau = \omega_0 t \quad d\tau = \omega_0 dt \quad (6.10)$$

Choosing  $\omega_0$  close to the limit cycle frequency will make the drawing of the phase-plane easier as the limit cycle curve will be almost circular. The time scaling transforms equation (6.9) into

$$\frac{d^2 \ell}{d\tau^2} = \frac{1}{\omega_0^2} \cdot \frac{L_{vn} \tan B}{m} \cdot e \quad (6.11)$$

For convenience, and to conform with standard usage, the following phase variables are defined

$$x_1 \triangleq \ell \quad (6.12)$$

$$x_2 \triangleq \frac{d\ell}{d\tau} \quad (6.13)$$

With the change in variables, equation (6.11) becomes

$$\frac{dx_2}{d\tau} = \frac{1}{\omega_0^2} \cdot \frac{L_{vn} \tan B}{m} \cdot e \quad (6.14)$$

Dividing equation (6.14) by  $x_2$  gives

$$\frac{dx_2}{dx_1} = \frac{1}{\omega_0^2} \cdot \frac{L_{vn} \tan B}{m} \cdot e \quad (6.15)$$

For the construction of the phase-plane equation (6.15) is rearranged to yield

$$x_2 = \frac{1}{\omega_0^2} \cdot \frac{L_{vn} \tan B}{m} \cdot \frac{e}{\frac{dx_2}{dx_1}} \quad (6.16)$$

which is the equation for the isoclines or loci of constant slope  $dx_2/dx_1$ . In

this case the isoclines are horizontal lines.

The value of  $e$  is determined by  $l_f$ , which is a function of  $x_1$  and  $x_2$ .

The first block of Fig. 6.4 gives

$$l_f = l + \frac{S_n}{V_n} \cdot \frac{dl}{dt} \quad (6.17)$$

Substituting equations (6.12) and (6.13) into equation (6.17)

$$l_f = x_1 + \omega_0 \frac{S_n}{V_n} x_2 \quad (6.18)$$

The value of  $e$  is then given by

$$e = 1 \text{ if } \begin{cases} l_f > l_m \\ l_m > l_f - l_m \text{ and } dl_f/dt > 0 \end{cases} \quad (6.19)$$

$$e = -1 \text{ if } \begin{cases} l_f > l_m \\ l_m > l_f > -l_m \text{ and } dl_f/dt < 0 \end{cases}$$

By use of equations (6.16), (6.18), and (6.19), it is now possible to construct phase-plane portraits for any point along the trajectory. Two points have been selected  $\bar{V} = 0.90$  and  $\bar{V} = 0.30$  and phase-plane curves have been drawn to show the limit cycles. The curves are shown in Fig. 6.5 and 6.6. The bank angle has been chosen so that  $\tan B = 0.5$  and the maximum allowable cross range error at the landing point has been set to  $l_m = 5\text{nm}$ .

The two phase planes in Fig. 6.5 and 6.6 have the important characteristic that the lateral control system always will settle down to the same stable limit cycle independent of initial conditions. A second important



$$x_2 = \frac{dl}{dt} \cdot \frac{1}{\omega_0}$$

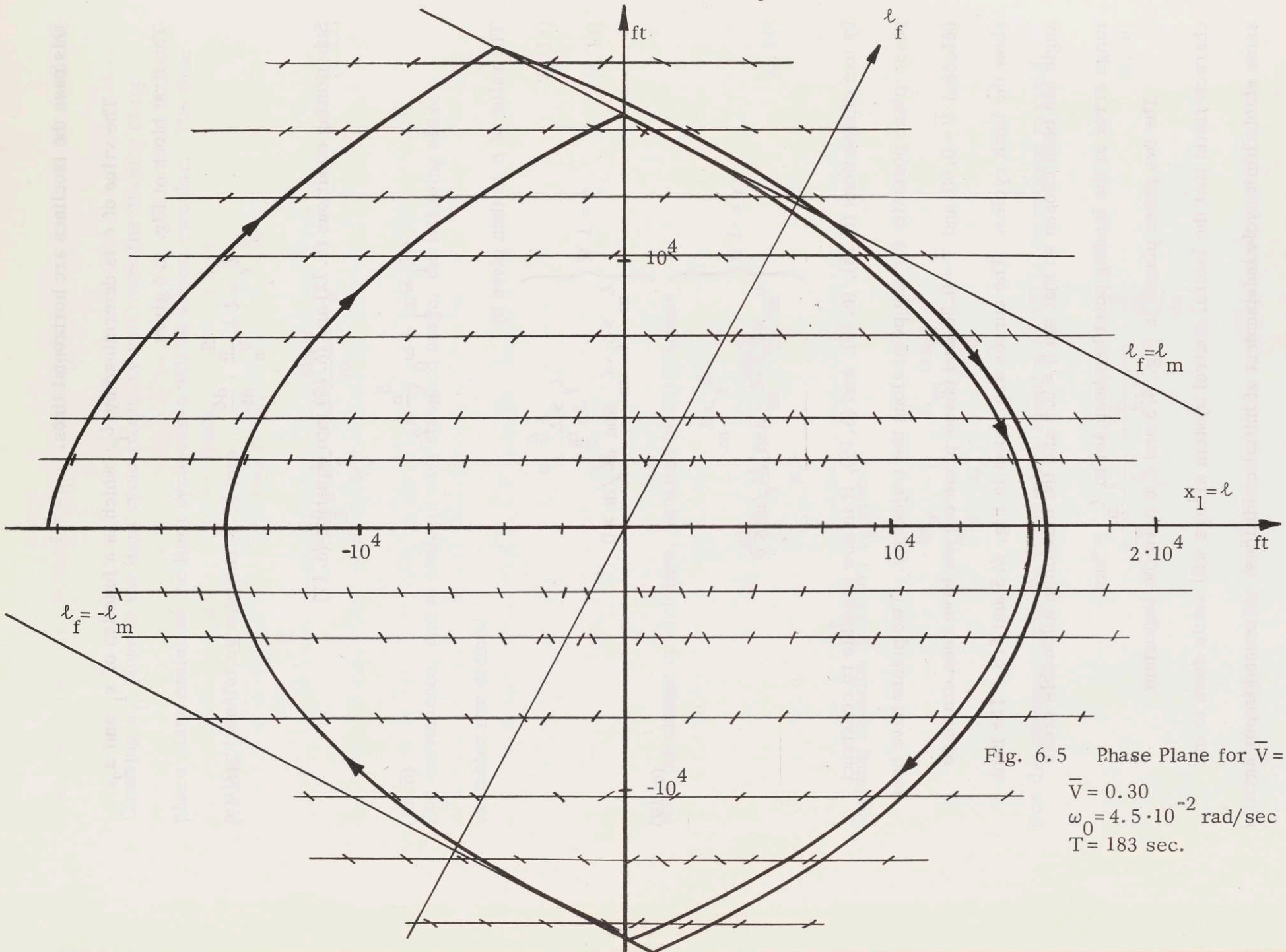


Fig. 6.5 Phase Plane for  $\bar{V} = 0.30$ .

$\bar{V} = 0.30$   
 $\omega_0 = 4.5 \cdot 10^{-2}$  rad/sec  
 $T = 183$  sec.

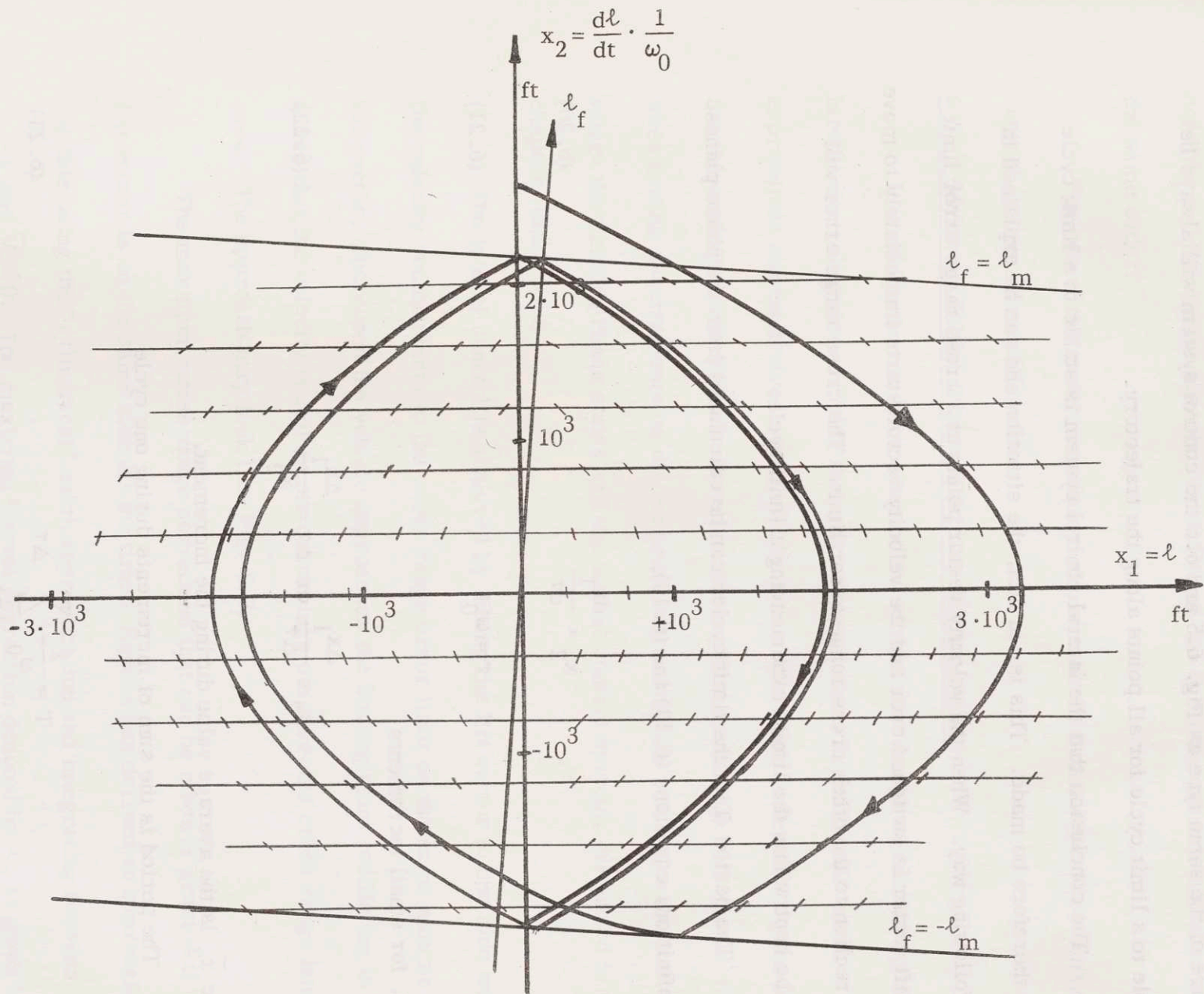


Fig. 6.6 Phase Plane for  $\bar{V} = 0.90$ .

$$\bar{V} = 0.90$$

$$\omega_0 = 5.5 \cdot 10^{-2} \text{ rad/sec}$$

$$T = 145 \text{ sec.}$$

characteristic is that the limit cycle always keeps the cross range error within the limits  $+\ell_m$  and  $-\ell_m$ . As the phase planes for points along the trajectory all are of the same type as Fig. 6.5 and 6.6 the control system will always be stable to a limit cycle for all points along the trajectory.

The conclusion that the lateral control system is stable to a limit cycle may therefore be made. This is, in fact, the situation and can be explained in the following way. When the velocity vector points at a cross range error limit the lift vector is switched over and the velocity vector starts immediately to move in direction to the other cross range error limit. The cross range error will thus be kept within the limits experiencing a limit cycle.

The period  $T$  of the limit cycles can be calculated from the phase planes. By definition, equations (6.13) and (6.10),

$$\dot{x}_2 = \frac{dx_1}{d\tau} \quad (6.20)$$

$$\tau = \omega_0 t \quad (6.21)$$

Thus, for small increments

$$\bar{x}_2 = \frac{\Delta x_1}{\Delta \tau} \quad \text{or} \quad \Delta \tau = \frac{\Delta x_1}{\bar{x}_2} \quad (6.22)$$

where  $\bar{x}_2$  is the average value during the increment.

The period is the sum of increments during one cycle

$$T = \frac{1}{\omega_0} \sum_{\text{one cycle}} \Delta \tau \quad (6.23)$$

Applying equation (6.23) to Fig. 6.5 and 6.6 gives  $T = 183$  sec. and

$T = 145$  sec. for  $\bar{V} = 0.30$  and  $\bar{V} = 0.90$ , respectively. It is surprising that the periods are so close as the control system is working under very different conditions. For points between  $\bar{V} = 0.90$  and  $\bar{V} = 0.30$  the periods are also of the same order.

Periods of the order, mentioned above, should fit the overall re-entry control system very well.

### 6.3 Maximum Initial Errors That Can Be Corrected

It is of interest to know what initial errors that can be corrected by the lateral control system. Using the approximation for a "cylindrical" earth, expressions can be derived which will be accurate enough to develop a good feeling for the capacity of the lateral control system. That knowledge will then be useful when setting requirements on the guidance controlling the vehicle to the point where the Landing Phase starts and the lateral control system, discussed in this chapter, takes over.

The lateral control is achieved by tilting the lift vector to one side until the velocity vector points to the cross range error limit on the same side as the lift vector, whereupon the vehicle approaches the landing point oscillating in such a way that the velocity vector never overswings the accepted cross range landing area. The approach may look like Fig. 6.7.

The maximum cross range correction that can be made is granted if the lift vector is on the same side all the time. Eggers has derived an expression for this using the "cylindrical" earth approximation and integrating between  $\bar{V}_i = 1$  and  $\bar{V}_f = 0$ . The maximum lateral correction denoted by  $l_0$  is given by

$$l_0 = \frac{\pi^2}{24} \cdot r \left( \frac{L}{D} \right)_v^2 \tan B \quad (6.24)$$

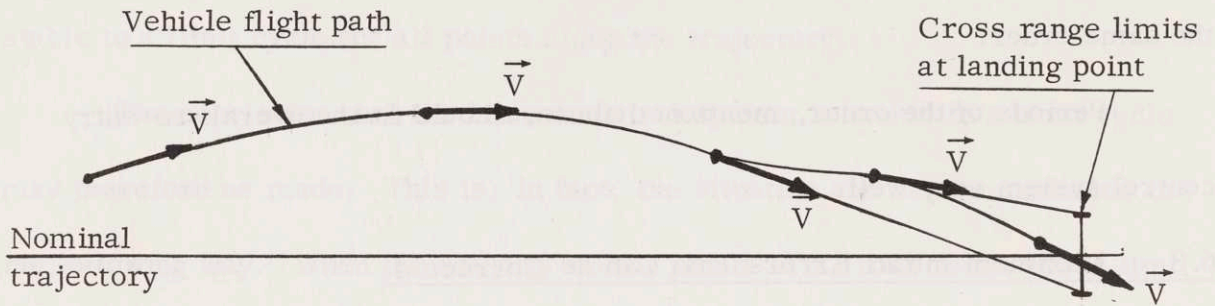


Fig. 6.7 Lateral Trajectory.

The cross range error that an unbanked vehicle would give at the landing point with the initial condition  $l_i$  and  $\psi_i$  at the beginning of the Landing Phase is shown in Fig. 6.8.

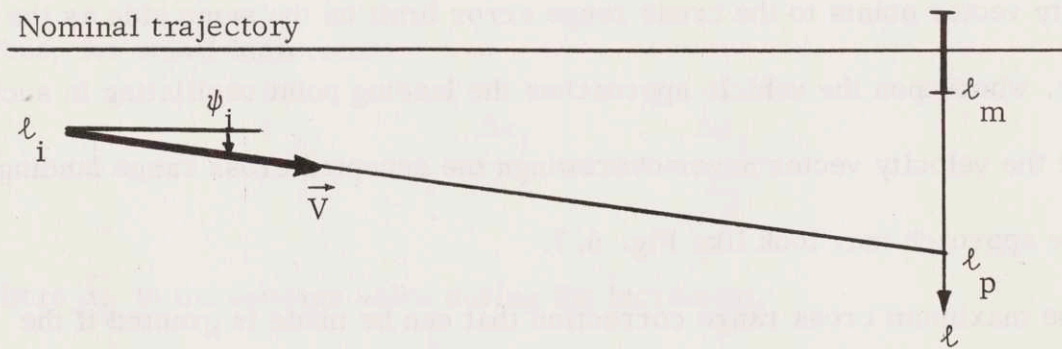


Fig. 6.8 Cross Range Error Due to Initial Errors.

Figure 6.8 gives the following predicted cross range error

$$l_p = l_i + S\psi_i \quad (6.25)$$

The initial conditions that can be corrected by the lateral control system are then

$$|\ell_i + \psi_i S| \leq \ell_m + \ell_0 \quad (6-26)$$

Substituting equations (2.16) and (6.24) into equation (6.26) yields

$$\left| \ell_i + \psi_i \cdot \frac{r}{2} \cdot \left(\frac{L}{D}\right)_v \ell_n \frac{1}{1-\bar{V}_i^2} \right| \leq \ell_m + \frac{\pi^2}{24} \cdot r \left(\frac{L}{D}\right)_v^2 \tan |B| \quad (6.27)$$

Equation (6.27) is graphically shown in Fig. 6.9 using the following values for the constants

$$r = 2.12 \cdot 10^7 \text{ ft}$$

$$\left(\frac{L}{D}\right)_v = 0.5$$

$$\tan |B| = 0.5$$

$$\bar{V}_i = 0.99$$

$$\ell_m = 3 \cdot 10^4 \text{ ft}$$

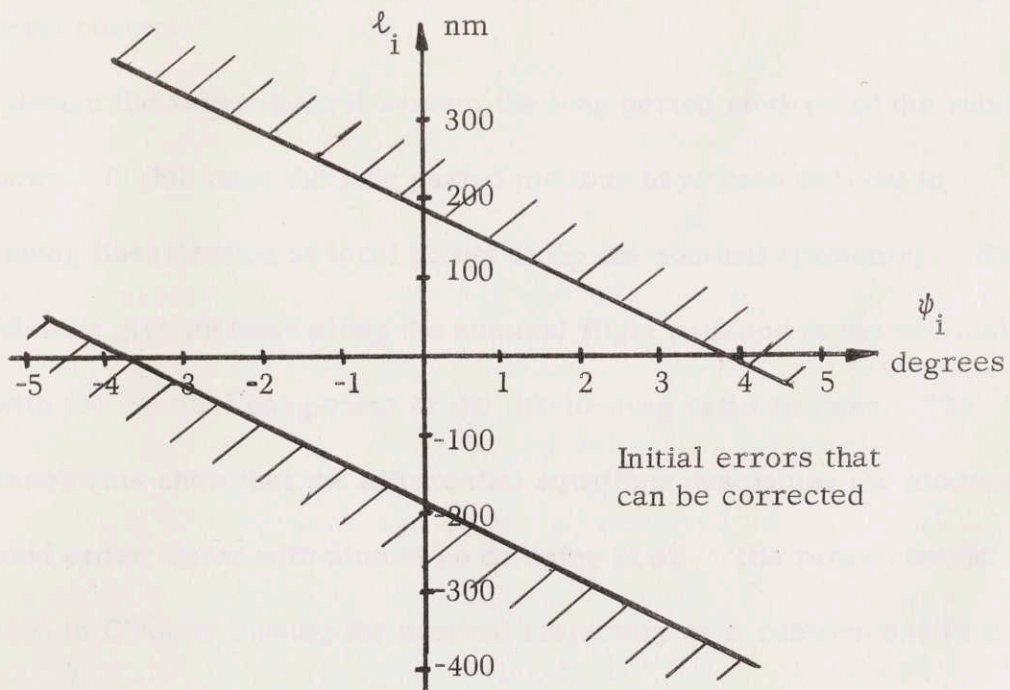


Fig. 6.9 Acceptable Initial Errors.

Initial errors in position and direction that can be corrected by the lateral control are in the area between the two straight lines in Fig. 6.9. That gives the requirements on the control before the Landing Phase.

In most guidance systems the position error is less important than the direction error of the velocity vector. The cross range limit  $l_m$  is also small compared to  $l_0$ . If  $l_i$  and  $l_m$  are neglected, equation (6.27) is transformed into the following handy formula

$$|\psi_i| \leq \frac{\pi^2}{12} \cdot \frac{\left(\frac{L}{D}\right)_v}{l_n \frac{1}{1 - \bar{V}_i^2}} \cdot \tan |B| \quad (6.29)$$

The upper limit for the initial angle error is proportional to the vertical component of the ratio lift to drag and the tangent of the bank angle.



## CHAPTER 7

### SUMMARY AND CONCLUSIONS; SUGGESTIONS FOR FURTHER STUDY

#### 7.1 Summary and Conclusions

This work has been concerned with the problem of controlling a lifting reentry vehicle through the atmosphere after the velocity has decreased to sub-circular. A simple approximate expression for the range is derived for a constant L/D ratio assuming that the trajectory is in a plane including the center of the earth. The range to go is shown to be proportional to the vertical component of the lift-to-drag ratio.

The control problem is divided into two problems. The range control and the lateral control.

To design the range control system the long period motions of the vehicle must be known. In this case the long period motions have been derived in Chapter 3 using linearization at local points along the nominal trajectory. The final expressions give motions along the nominal flight path and in the vertical direction with the vertical component of the lift-to-drag ratio as input. The Laplace-transforms show that the differential equations describing the motions have a second order factor with almost no damping at all. The range control loop is closed in Chapter 5 using the nominal trajectory as a reference with time as independent variable. The differences between actual state and reference state



are used to control the vertical component of the lift-to-drag ratio. The acceleration and velocity along the flight path are included to damp and stabilize the system.

The delta-modulated accelerometer is described in Chapter 4. Its output consists of pulses each of them representing an incremental increase of measured velocity. The two-level and three-level relay accelerometer is analyzed for modes and finally a non limit cycling delta-modulated accelerometer is designed for use in the range control loop. When eliminating the modes of the delta-modulated accelerometer both the high energy and the low energy regions are analyzed. It is found that the low energy region defines the width of the zero level of the three level relay in accelerometers with small  $\tau/T_s$ . Further, a non-linear model is derived describing the low frequency behaviour of the accelerometer.

The delta-modulated accelerometer is applied to the range control loop. The loop is then analyzed for limit cycles caused by the output character of the accelerometer. Only at the beginning of the Landing Phase does the range control loop experience a limit cycle. There will, therefore, be no range errors caused by the limit cycling analyzed.

The lateral control system is described in Chapter 6 and switches the lift vector fast from one side to the other every time the velocity vector of the vehicle points towards one of the limits for the cross range error at the landing point. The lift vector has from the stand point of the lateral control system only two positions. To the left or right of the vertical plane with the same vertical component of lift. The magnitude of the vertical component is determined by the range control system and is close to the nominal value. Thus,

the lateral control system acts as an on-off system and the limit cycles have been analyzed using the phase plane method.

## 7.2 Suggestions for Further Study

The work in this thesis has been directed towards limit cycle analysis and the next step on that way is to include the roll angle control and the quantization of the DDA computer in the analysis.

The cross coupling between the lateral and range control systems should also be added to the study of a reentry control system. A complete design of a reentry control also requires a study of the initial errors that the control system can handle without exceeding the limits of the vehicle and what the crew can stand.

A comparison of a range control system using time as independent variable and one using velocity as independent variable could give useful information about which choice is the best. Other methods for the range control system should be tried.

## REFERENCES

1. Rosenbaum, Richard, Landing Point Control for a Lifting Vehicle Entering a Planetary Atmosphere, Sc.D. Thesis, M. I. T., Aero. Dept., 1961.
2. Slye, Robert E., "An Analytical Method for Studying the Lateral Motion of Atmosphere Entry Vehicles," NASA TN D-325, September 1960.
3. Wiener, Thomas F., Theoretical Analysis of Gimballess Inertial Reference Equipment Using Delta-Modulated Instruments, Sc.D. Thesis, M. I. T., Aero. Dept., 1962.
4. Monroe, Alfred J., Digital Processes for Sampled Data Systems, John Wiley and Sons, Inc., New York, 1962.
5. Vander Velde, Wallace E., "Computers in Inertial Navigation Systems," Section V in Inertial Guidance-Terrestrial and Interplanetary, (Course Notes for 16.45S, M. I. T., Summer, 1960).
6. Forbes, George F., Digital Differential Analyzers, Own Publication, 10117 Barke Avenue, Pacoima, California, 1956.
7. Chapman, Dean R., "An Approximate Analytical Method for Studying Entry into Planetary Atmospheres," NASA TR R-11, 1959.
8. Wingrove, Rodney C., "A Study of Guidance to Reference Trajectories for Lifting Reentry at Supercircular Velocity," NASA TR R-151, 1963.
9. Wingrove, Rodney C., "Survey of Atmosphere Re-Entry Guidance and Control Methods," AIAA Journal, Vol. 1, Number 9, September, 1963.
10. Bliss, G. A., Mathematics for Exterior Ballistics, John Wiley and Sons, Inc., New York, 1944.
11. Tsien, H. S., Engineering Cybernetics, McGraw-Hill Book Company, Inc., New York, 1955.
12. Torng, H. C., and Meserve, W. E., "Determination of Periodic Modes in Delay Servomechanisms Employing Sampled Data," IRE Transactions on Automatic Control, September 1960, pp. 298-305.

## REFERENCES

13. Bergen, A. R., "Discussion," following Torng and Meserve's paper, Ref. 12, IRE Transactions on Automatic Control, September, 1960, p. 304.
14. Chow, C. K., "Contactor Servomechanisms Employing Sampled Data," Transactions AIEE, Part II, LXXIII (1954), pp. 51-64.
15. Russell, Frederick A., Design Criterion for Stability of Sampled Data On-Off Servomechanisms, Ph. D. Thesis, Columbia University, 1953.
16. Eggers, A. J., "The Possibility of a Safe Landing," Chapter 13, Space Technology, John Wiley and Sons, Inc., New York, 1959.
17. Kalman, Randolph E., Phase Plane Analysis of Non-Linear Sampled Data Systems, S. M. Thesis, M. I. T., 1954.